Article

Proposed Methodology for Accuracy Improvement of LOD1 3D Building Models Created Based on Stereo Pléiades Satellite Imagery

Ana-Ioana Breaban [1], Valeria-Ersilia Oniga [2,*], Constantin Chirila [2], Ana-Maria Loghin [3], Norbert Pfeifer [3], Mihaela Macovei [2] and Alina-Mihaela Nicuta Precul [4]

[1] Department of Terrestrial Measurements and Cadastre, Faculty of Geodesy, Technical University of Civil Engineering Bucharest, Teiul Doamnei Street, 023585 Bucharest, Romania

[2] Department of Terrestrial Measurements and Cadastre, Faculty of Hydrotechnical Engineering, Geodesy and Environmental Engineering, "Gheorghe Asachi" Technical University of Iasi, Professor Dimitrie Mangeron Boulevard 67, 700050 Iași, Romania

[3] Department of Geodesy and Geoinformation, Technische Universität Wien, Karlsplatz 13, 1040 Vienna, Austria

[4] Department of Concrete Structures, Building Materials, Technology and Management, Faculty of Civil Engineering and Building Services, "Gheorghe Asachi" Technical University of Iasi, Professor Dimitrie Mangeron Boulevard 67, 700050 Iași, Romania

* Correspondence: valeria-ersilia.oniga@academic.tuiasi.ro; Tel.: +40-745-634-472

Abstract: Three-dimensional city models play an important role for a large number of applications in urban environments, and thus it is of high interest to create them automatically, accurately and in a cost-effective manner. This paper presents a new methodology for point cloud accuracy improvement to generate terrain topographic models and 3D building modeling with the Open Geospatial Consortium (OGC) CityGML standard, level of detail 1 (LOD1), using very high-resolution (VHR) satellite images. In that context, a number of steps are given attention (which are often (in the literature) not considered in detail), including the local geoid and the role of the digital terrain model (DTM) in the dense image matching process. The quality of the resulting models is analyzed thoroughly. For this objective, two stereo Pléiades 1 satellite images over Iasi city were acquired in September 2016, and 142 points were measured in situ by global navigation satellite system real-time kinematic positioning (GNSS-RTK) technology. First, the quasigeoid surface resulting from EGG2008 regional gravimetric model was corrected based on data from GNSS and leveling measurements using a four-parameter transformation, and the ellipsoidal heights of the 142 GNSS-RTK points were corrected based on the local quasigeoid surface. The DTM of the study area was created based on low-resolution airborne laser scanner (LR ALS) point clouds that have been filtered using the robust filter algorithm and a mask for buildings, and the ellipsoidal heights were also corrected with the local quasigeoid surface, resulting in a standard deviation of 37.3 cm for 50 levelling points and 28.1 cm for the 142 GNSS-RTK points. For the point cloud generation, two scenarios were considered: (1) no DTM and ground control points (GCPs) with uncorrected ellipsoidal heights resulting in an RMS difference (Z) for the 64 GCPs and 78 ChPs of 69.8 cm and (2) with LR ALS-DTM and GCPs with corrected ellipsoidal height values resulting in an RMS difference (Z) of 60.9 cm. The LOD1 models of 1550 buildings from the Iasi city center were created based on Pléiades-DSM point clouds (corrected and not corrected) and existing building sub-footprints, with four methods for the derivation of the building roof elevations, resulting in a standard deviation of 1.6 m against high-resolution (HR) ALS point cloud in the case of the best scenario. The proposed method for height extraction and reconstruction of the city structure performed the best compared with other studies on multiple satellite stereo imagery.

Keywords: stereo Pléiades images; local quasigeoid; 3D building model; LOD1; urban area

1. Introduction

Geospatial data, both two-dimensional (2D) and three-dimensional (3D) data, play a key role in determining and creating the infrastructure of an anthropic area. Three-dimensional city models are the most important, as they are used as a base for the smart city concept in implementing high technology in the urban environment and also by local governments for identifying changes, dynamic processes monitoring, urban planning. etc. [1,2]. Smart city development has drawn upon the development of specific abilities, namely scientific and technical abilities, proper management or political–administrative abilities, explaining it and thus justifying 3D city modeling as a research theme [3]. With the main purpose of creating a three-dimensional city model, the digital surface model (DSM) represents one of the most important aspects providing the geometry and structure of an urban environment with buildings being the most prominent objects in it as, over time, new buildings are being built, existing ones are expanded and old buildings are torn down [4]. Conventional ground surveying, stereo airborne or satellite photogrammetry, interferometric synthetic aperture radar (InSAR) and light detection and ranging (LiDAR) are the main data sources and technologies used to obtain high-resolution elevation information. Since the launch of the IKONOS satellite in September 1999, the number of VHR optical satellites has been increasing, bringing users many advantages such as a ground resolution of less than 1 m, a high temporal resolution and the acquisition of multiple images of the same area from different angles ensuring a stereoscopic coverage which is an essential aspect for 3D information generation.

Over large built-up areas such as the urban environment, the processing of space-borne optical sensor data (WorldView 1/2/3/4, GeoEye-1, IKONOS, Cartosat) allowed the reconstruction of 3D building modes at the city scale [5,6] at LOD1 and LOD2. LOD describes the degree of detail of geometry; objects become more detailed with increasing LOD. CityGML version 3.0 refines the concept of LOD by removing the LOD4 that is used for indoor modeling and integrating it in LODs 0 to 3 [7]. The level of detail LOD1 allows the 3D reconstruction of the buildings by a simple estimation of the heights without modeling the structure of the roof, this being considered flat. So, the real-world geometry of a building can be spatially represented by a 3D solid [8]. An essential part of deriving the 3D LOD1 reconstruction of the buildings is to extract the height of the buildings from the DSM point cloud automatically obtained by dense image matching. Image matching handles finding the correspondences between two or more images and is the most important process in the field of digital photogrammetry and computer vision [9] used for bringing two images in agreement, 3D reconstruction or re-localization [10]. Different image matching approaches are being used for DSM/DTM point cloud generation from VHR satellite images or aerial images: least squares matching (LSM), semi-global matching (SGM), normalized cross-correlation (NCC), feature-based matching (FBM), cost-based matching (CBM), etc. An existing digital elevation model (DEM) can be used for automatic aerial triangulation and/or 3D reconstruction by dense image matching. In the case of aerial triangulation, it is recommended to use an existing DEM for height initialization on very mountainous terrain, while in the case of other area types such as flat or hilly terrain, a mean terrain height can be specified, but with an accuracy of 50–100 m [11]. Good starting values for the correct height of each image are important; the best option as recommended in [11] would be an accurate DEM.

In this study, we present a methodology for the accuracy improvement of 3D building models created based on stereo Pléiades satellite imagery, having as the main step the use of an accurate DTM in the dense image matching process of stereo Pléiades satellite imagery. In addition, the impact of the DTM on the dense image matching process for deriving DSM and DTM point clouds, together with the use of Pléiades-DSM point clouds for automatic creation of the LOD1 building 3D models in a GIS environment, is analyzed. For 3D building reconstruction, a prismatic model at LOD1 was chosen starting from existing buildings sub-footprints, each one representing a specific building part, and extrusion to the calculated height for each individual part of the building based on the Pléiades-DSM

point cloud. The solution of using existing buildings sub-footprints was chosen because, as also mentioned in [12], the DSM point clouds generated from satellite images are affected by mismatches, blunders or missing values resulting in less accurate building footprint detection, their geometry being influenced by artifacts. This method is simple and can produce 3D models of complex buildings at LOD1 for an entire city.

1.1. Related Work

Regarding the process of 3D building reconstruction based on VHR satellite images, the state of the art has quite a few scientific papers. The potential of stereo and tri-stereo Pléiades satellite images was tested in the last decade for obtaining DEMs [13–19], DSMs [5,13,20–23] or automatic building extraction at LOD1 or LOD2 [24–26]. In [24], the buildings are reconstructed in 3D at LOD1, the building footprints and the rooftop polygons are automatically extracted, and the height information of every building is obtained by subtracting the DTM from the DSM and retaining the median or the majority values. However, the quantitative evaluation of the DSM or the building heights was not performed using other data sources, such as an ALS point cloud. Only a theoretical elevation precision of 3.06 m is specified, obtained based on the satellite azimuth and elevation of each image of the stereo-pair. Three-dimensional building models obtained by 2D cadastral maps and simulated Pléiades stereoscopic triplets were evaluated in [25] against original 25 cm resolution aerial images, resulting in an RMSE for 467 buildings in an urban area of 70 cm. However, the results were not based on real images. The accuracy of 3D building reconstruction based on Pléiades-DSM was determined in [26] only by visual analysis using DSM profiles against ground truth obtained from aerial images, leading to the conclusion that the Pléiades-DSM presented the building edges and outlines as well as the areas between the high buildings. The vertical accuracy of the DSM was tested only based on 30 points, resulting in an RMSE of 60 cm.

A workflow for building 3D reconstruction from WorldView-2 satellite images was proposed by [27]. The height information was obtained from the height map (DSM-DTM) for the centroid of the building polygon, while the buildings' footprints were automatically extracted from the pan-sharpened image. Only the assessment of building footprints was performed together with a comparison between the DEM and the Space Shuttle Radar Topography Mission (SRTM), resulting in an RMSE of 5.98 m. A study on 100 buildings [6] tested the height reconstruction accuracy using a Pléiades tri-stereo DSM, obtaining a mean value for the height residuals of 2.02 m. In addition, in a study on 17 buildings, the mean of the residual values in height was 1.94 m for LOD2 reconstructed buildings from GeoEye DSM as reported in [5].

Considering the DTM and the DSM as the main dataset input for 3D building reconstruction, high importance should be given to the dense image matching process. So, several studies were conducted to test the point cloud accuracy obtained by different image matching algorithms [28–31], but, even if it is recommended to use an existing DEM in the dense image matching process of aerial or satellite images, the researchers did not focus on testing the quantitative impact of the DEM on the DTM/DSM point clouds in their studies.

In [9], the global SRTM is introduced in the image matching process to find the real elevation range in the neighborhood of each seed point. Comparing the results with two other methods. i.e., geometrically constrained cross-correlation (GC) and triangulation-based affine, adaptive cross-correlation (TAACC), the proposed method, by introducing the SRTM, reduces the mismatching rate to 0.6% and the RMSE to 2.4 m in contrast to GC with a mismatching error of 1.4% and an RMSE of 3.4 m and the TAACC with a mismatching error of 98.7% and an RMSE of 102 m. A new algorithm for image matching of Pléiades imagery is proposed by [13], named by the authors "truncated SGM", to speed up the process and to gain accuracy. The algorithm incorporates a coarse DEM (e.g., SRTM DEM, ASTER GDEM, World DEM) on the top pyramid level to calculate disparity predictions, thus limiting the search space and reducing the biases that cause incorrect reconstructions of surfaces.

1.2. Motivation for Creating and Using the Local Quasigeoid

GCPs and ChPs, usually with planimetric coordinates extracted for the orthophoto and the elevation from a LiDAR DTM [6,15], LiDAR-derived GCPs [5,16] or comparison with LiDAR point clouds [13,28–34], were used to test the accuracy of the Pléiades-derived products. Nevertheless, when comparing the results from different studies, we have to keep in mind that LiDAR measurements have an accuracy of between 15 and 25 cm [14] and will not have in situ measurement accuracy [13].

In order to have a clearer view of Pléiades stereo image processing workflow accuracy, for this study, all GCPs and ChPs have been measured in the field by GNSS-RTK technology, enabling quick survey performance. However, the quality of RTK measurements can be affected by ionospheric errors, tropospheric errors, signal obstructions and multipath errors [35,36] caused by features in the vicinity of the receiver [37] such as tree canopies and high buildings. For points with a high level of obstruction, the RTK measurements lead to decimeter-level accuracy, as reported in [36]. In addition, there is a high correlation between the number of tracked satellites and high accuracy [36] and a high correlation between the distance from the rover to the GNSS base stations and the base station coordinate accuracy [38], a number of 20 GNSS satellites was found to lead to higher position accuracy against 12 satellites for both static and RTK surveys [36]. The literature mentioned that for distances less than 1 km from the base station to the rover, elevation differences determined by GNSS can usually be assumed to be normal height differences, the errors being typically around the 3 cm range, while for distances less than 10 km, the errors are within 3–10 cm [39]. Yet, as there are so many critical factors affecting the RTK accuracy, this should be not considered a general rule.

In conclusion, for the GNSS-RTK technology to meet geodetic standards, it is of high importance to apply correction surfaces (local geoid model) to RTK ellipsoidal heights in order to remove systematic errors and increase their reliability [40].

Currently, in Romania, a differentiated model is applied for the transformation of the ellipsoidal heights from the ETRS89 European datum into Black Sea-1975 normal heights, corresponding to the RO Const/NH vertical datum [41]. Coordinate transformation is performed in a unitary and homogeneous manner through the TransDatRO software (ver. 4.07) made available by the National Agency for Cadaster and Land Registry (NACLR). The counties for which the gravimetric quasigeoid was generated with a global precision of ±10–12 cm are located in the western, southern and central areas of the country (Figure 1a). Otherwise, a determined geometric quasigeoid based on the European gravimetric quasigeoid model (EGG97) and GNSS/leveling measurements with an estimated accuracy of ±15–50 cm was used [42]. Given the need for improved accuracy in transforming heights in areas not yet covered by gravimetric measurements, for the Iasi city located in the northeastern region of Romania, this study chose to create a correction surface of the regional quasigeoid using dense GNSS/leveling points belonging to the geospatial control network. Thus, compared to the previous version of the European quasigeoid (EGG97) used in the TransDatRO software, a more recent version (EGG2008) offering a '1 × 1' spacing grid for the ellipsoidal height anomalies was chosen (Figure 1b). The grid limits were set for a latitude between 47°05′ and 47°13′, and for a longitude between 27°29′ and 27°42′.

Since the 3D models of topography, especially the 3D city models, are used together with diverse data sources, it is necessary to apply a certain level of rigorousness and feasibility. Therefore, to correct the ellipsoidal heights of the GCPs and ChPs measured in situ by GNSS-RTK technology and also to obtain an accurate DTM of the hilly terrain of the study area, the solution was to use the local quasigeoid for the city of Iasi, which is superior to the gravimetric quasigeoid as stated by [43].

1.3. Research Methodology

To the best of our knowledge, no study tested the accuracy of the Pléiades DSM/DTM point clouds using the leveling measurements or the quantitative impact of the DTM on the 3D reconstruction process if introduced in the main processing workflow; this study

represents the first initiative of implementing satellite photogrammetry based on Pléiades HR stereo imagery to derive a refined DSM suitable for smart city applications.
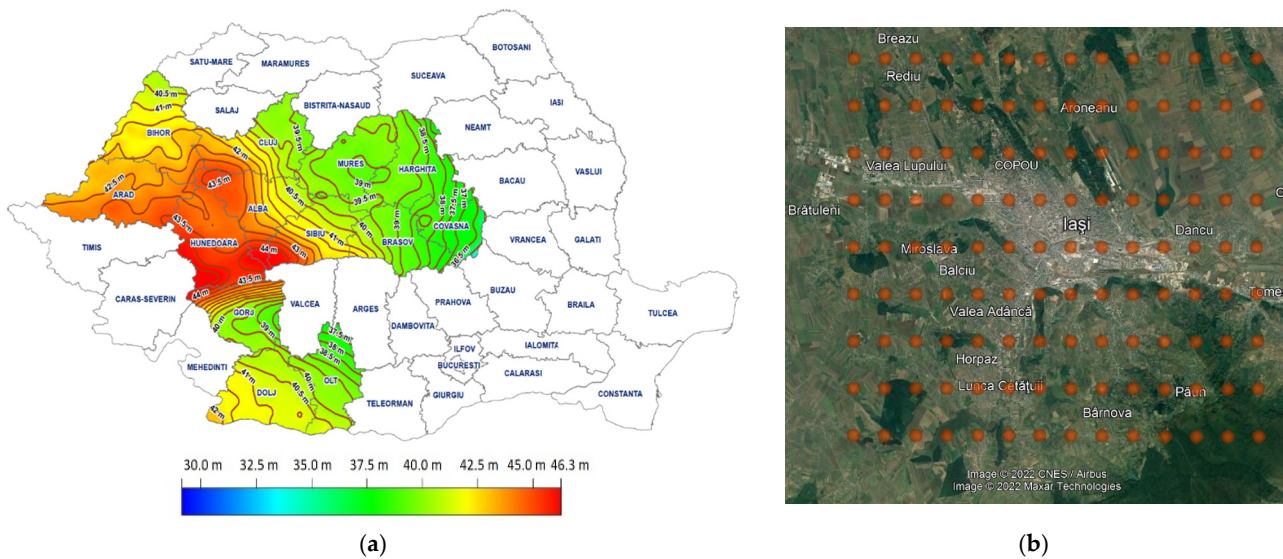

(**a**)

(**b**)

Figure 1. (**a**) Gravimetric quasigeoid for the Romanian territory; (**b**) EGG2008 grid extracted for the Iasi city study area.

Specifically, our research study has the main purpose of finding the answers to the following questions: (1) What is the quantitative impact of the DTM in the process of dense image matching of a stereo-pair of Pléiades satellite images on the accuracy of the derived DTM and DSM point clouds and (2) on LOD1 building 3D model accuracy? (3) What is the accuracy of the DTM and DSM point clouds derived from a single stereo-pair of Pléiades images against leveling measurements? (4) What method for building height calculation gives the best results for LOD1 building 3D model reconstruction? To answer these questions, we used two sets of stereo Pléiades satellite imagery over a ~90 km^2 study area, located in the northeastern part of Romania. The absolute vertical accuracy of the photogrammetrically derived DTMs and DSMs is evaluated against 142 points measured using GNSS-RTK technology and leveling points from the geospatial control network of Iasi city, using two different scenarios: (1) no DTM and GCPs and ChPs with uncorrected ellipsoidal heights (uncorrected scenario) and (2) with LR ALS-DTM and GCPs and ChPs with corrected ellipsoidal heights (corrected scenario).

The workflow of the research methodology is presented in Figure 2.

Our contributions can be summarized as follows:

1. Using a very high number of ground control points (GCPs) and check points (ChPs), i.e., 142, to process the Pléiades images, all of them being measured in the field using GNSS-RTK technology, the vertical accuracy of DTMs and DSMs extracted from the small-convergence-angle stereo-pair being significantly improved.

2. Improving the accuracy on the elevation of the dense image matching process calculated based on GCPs and ChPs leading to a 9 cm better accuracy, by correcting the LR ALS-DTM and the GNSS-RTK measurements with the local quasigeoid.

3. Improving the accuracy of the Pléiades-DSM point cloud by introducing the DTM in the process of dense image matching, the systematic errors caused by buildings and vegetation being considerably reduced.

4. Validation of four methods for deriving the building roof elevations: (i) calculating the mean and median heights for the points inside the building footprint; (ii) computing the centroid for which the elevation was interpolated in the Pléiades-DSM point cloud; (iii) calculating the elevation of the centroid in a buffer of 1 m radius through interpolation in the DSM point cloud; (iv) calculating the mean and median heights

for the points inside the building footprint, modified with an interior buffer of 1 m to eliminate the facade points.
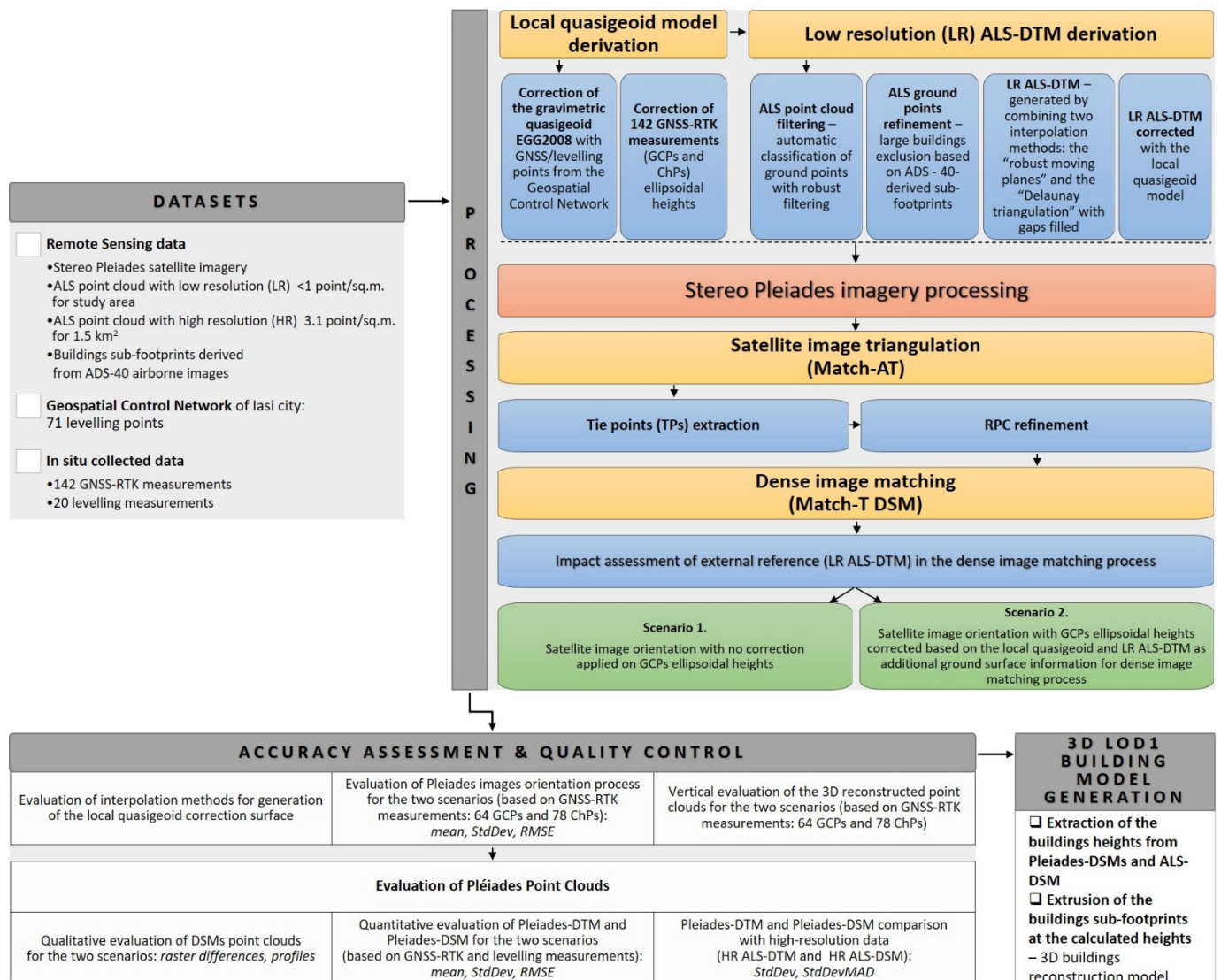

Figure 2. Flow chart of research methodology.

2. Study Area and Data Analysis

2.1. Study Area

The objective of the present study is to investigate the potential of the extraction of an accurate DSM of a hilly urban area through satellite photogrammetry. So, a hilly dense cityscape was chosen for this case study, representing the city of Iasi located in the northeastern part of Romania (47°09′06″N; 27°35′16″E; WGS84). By its extension, Iasi is the legendary "city of the 7 hills", described in 1691 by the Italian Marco Bandini as "a new Roma" with elevations ranging from 40 m to 400 m. Covering an area of 94 km², the city of Iasi is a university town, the second most populous city in Romania and the home of extraordinary national heritage values (Figure 3).

2.2. Stereo Pléiades Satellite Images

The Pléiades 1 mission consists of a constellation of two satellites, 1A/1B, for VHR panchromatic (PA) and multispectral (MS) optical observation of the Earth's surface at nominal resolutions of 0.5 m and 2 m, respectively. The stereo Pléiades images were ordered at the sensor geometric processing level; the product was extracted from one strip

acquisition based on a polygonal region of interest, i.e., the generalized administrative limit of Iasi in WGS84 coordinates, and the pixels outside the polygon were black-filled. This geometric processing level includes the correction of instrumental and optical distortions, such as the viewing angles adjusted to the single linear array model and the refinement of attitudes and ephemeris data [44]. For each satellite image, the RPCs are provided with the product, enabling the transformation from image coordinate system to object coordinate system, in this case, the Romanian national coordinate system "Stereographic on a unique secant plane-1970" (STEREO-70). For the spectral band combination, the bundle option was specified, the panchromatic and the multispectral products being simultaneously acquired but delivered separately, i.e., one file for multispectral and one file for panchromatic. The main acquisition parameters of the stereo Pléiades images are summarized in Table 1.
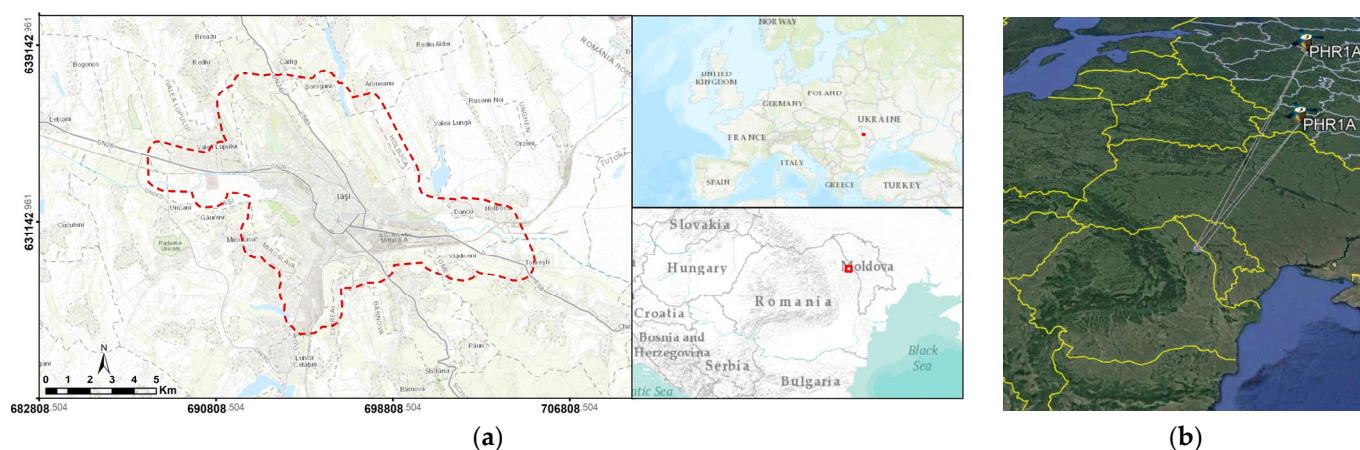

(a)   (b)

Figure 3. (**a**) Location of the study area; (**b**) acquisition geometry of stereo Pléiades satellite images.

Table 1. Acquisition parameters of stereo Pléiades images.

Sensor Type & Acquisition Date	View	Acquisition Time (hh:hm:ss.s)	Incidence Angles (∘)			B/H Ratio
			Across	**Along**	**Global**	
Pléiades	Forward (F)	09:05:45.031250	−14.169	−12.182	20.659	0.39 (FB)
7 February 2016	Backward (B)	09:06:22.031250	18.037	−5.539	18.766	

For the panchromatic images used further in this case study, an optical radiometric calibration was performed using the open-source software Orfeo Tool Box [45], the pixel values being calibrated with the parameters described in [6]. As listed in Table 1, the stereo Pléiades images were acquired on the morning of 7 February 2016 within 37 s. The distance traveled by the satellite was 270.05 km. The images have a B/H ratio of 0.39 and an intersection angle of rays on the ground of 19°, which is a small convergence angle according to [13].

The two radiometrically corrected Pléiades panchromatic images are shown in Figure 4, and a detail view is shown in Figure 5.

2.3. LR ALS Measurements

The LR ALS flight was completed in March 2012, the beneficiary being the Water Basin Agency Prut-Bîrlad, Romania, and comprised a total of 600 bands acquired with the Leica ALS50 sensor and a wavelength of 1064 nm. The system acquisition speed was 57 m/s, the flight height was 1600 m and the field of view (FOV) was 45°, ensuring a strip width of 1325 m. The LR ALS point cloud density is 0.03 points/sqm, and the coordinate reference system is UTM 35 North, datum WGS 84. From the total of 600 strips, 29 were selected for the Iasi city and clipped following the Pléiades satellite image simplified boundary using

the ArcGIS software (Figure 6a). The LR ALS point clouds have high noise as can be seen in Figure 6b due to scattering in the atmosphere.
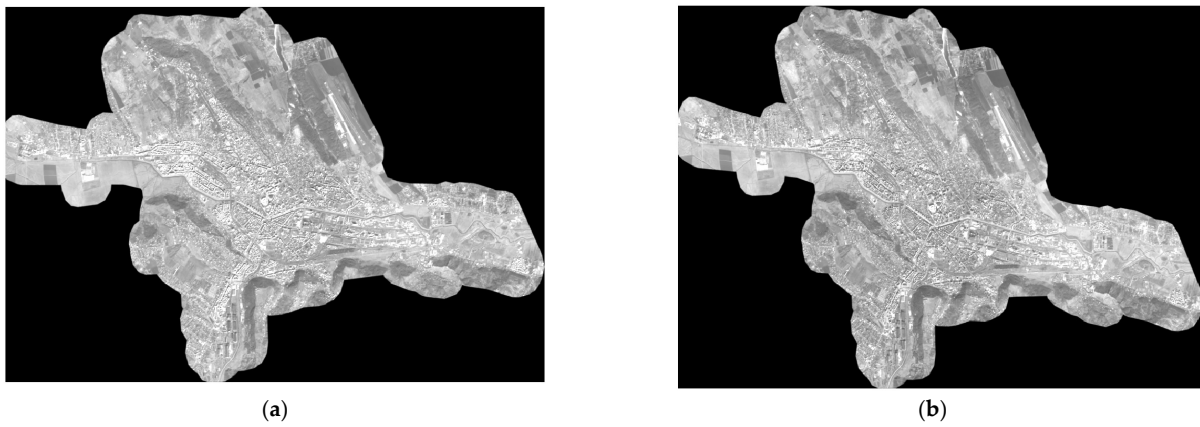

(**a**)　　　　　　　　　　　　　　　　　　　　　　　　　　　(**b**)

Figure 4. Pléides panchromatic satellite images: (**a**) forward-looking image; (**b**) backward-looking image.

(**a**)　　　　　　　　　　　　　　　　　　　　　　　　　　　(**b**)

Figure 5. Detail of Pléiades satellite images in panchromatic band on the same area: (**a**) forward-looking image, (**b**) backward-looking image.
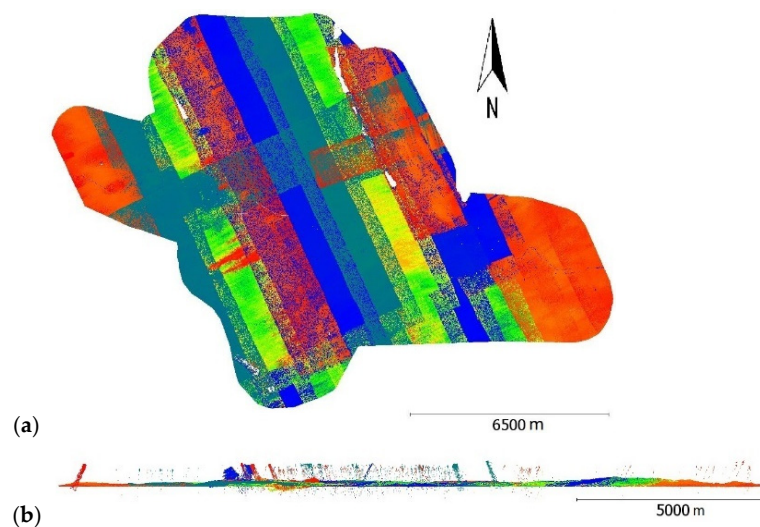

(**a**)

6500 m

(**b**)

5000 m

Figure 6. The LR ALS original strips along the Iasi city area: (**a**) top view; (**b**) front view.

2.4. Leveling Points of the Geospatial Control Network

The geospatial control network was designed and executed in 2005 for the introduction of the urban cadastral survey in Iasi city. GNSS measurements were performed in static

mode and led to accuracies of ellipsoidal heights of ±2–3 cm. On the other hand, the leveling measurements were carried out in the form of polygonal traverses, resulting in millimeter accuracies for the Black Sea-1975 normal heights of the new points [46]. The geospatial control network consists of 71 leveling points (Figure 7a) marked by metallic bold markers encapsulated in metallic shields (Figure 7b) or in concrete (Figure 7c) and embedded in the ground surface, of which 9 are located outside the study area.
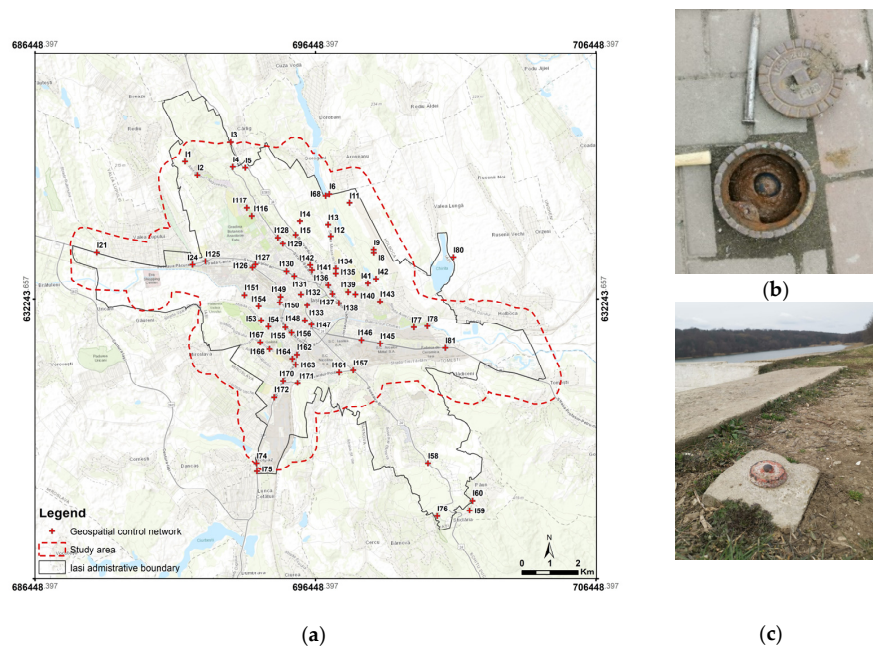

(a)   (b)   (c)

Figure 7. (**a**) Geospatial control network of 71 leveling points; (**b**) metallic survey markers; (**c**) concrete survey markers.

2.5. GNSS-RTK Measurements for Ground Control Points and Check Points

For this study, a total of 142 points have been chosen for the role of GCPs and ChPs. In this regard, a grid of 2 km size was applied to be a guideline to manually choose these points following three rules: to be visible on the Pléiades images, to be situated in areas that did not suffer changes during the period of 2016 (year of image acquisition) to 2021 (year of GNSS-RTK measurements) and each grid cell to have at least one point so that they would be uniformly distributed over the Iasi city area (Figure 8).

Figure 8. The location of GNSS-RTK measurements over the study area.

In order to be visible on the images, road intersections (Figure 9a), crosswalks (Figure 9b), parking markings (Figure 9c) or corners of paved areas were chosen as GCPs and ChPs. The 142 points were measured in approximately two weeks by GNSS-RTK technology in July 2021.
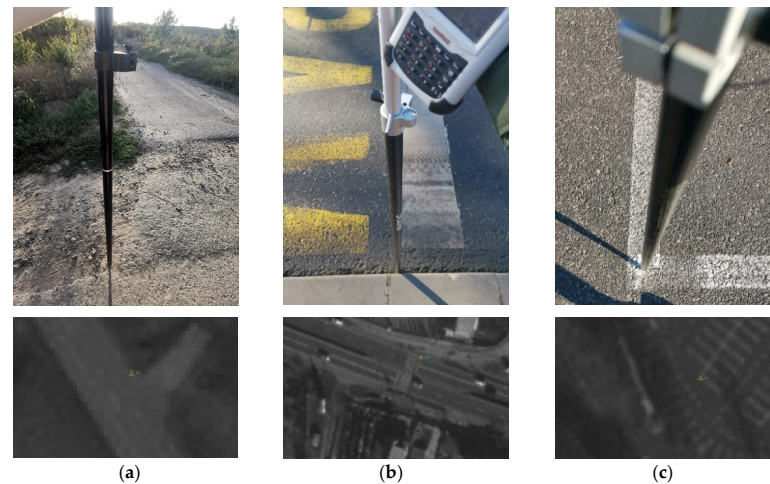

(**a**)   (**b**)   (**c**)

Figure 9. The location of GNSS-RTK measurements in the field and on images: (**a**) road intersection; (**b**) crosswalk and (**c**) parking markings.

The measurements were performed with a South S82-T GNSS receiver with double frequency using the Romanian Positioning Determination System (ROMPOS) that ensures precise positioning in the European Terrestrial Reference System 1989 (ETRS89) [38] using GNSS-RTK technology. This technique allows surveyors to perform surveys quickly [36] and in a more efficient way. Two types of products can be accessed through real-time positioning services: nearest (single-base RTK) with the use of differential corrections from a single reference station, and network RTK that involves the calculation of corrections based on the closest observation reference stations around the user [38]. For this case study, the Nearest_3.1 option was used, so all observations received differential corrections from the Iasi GNSS permanent station, the distances between the measured points and the station being in the range of 300 m to 9.4 km as can be seen in Figure 10.
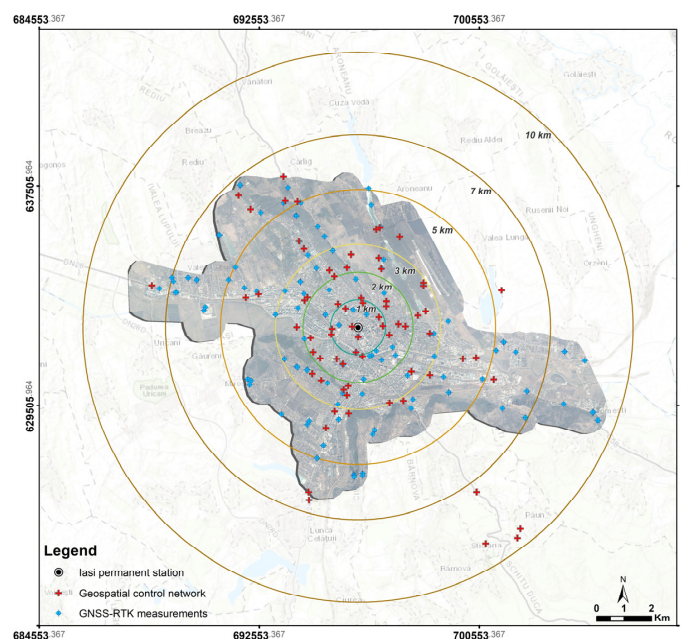

Figure 10. GNSS measurements for GCPs and ChPs (blue) and leveling points (red).

The planimetric transformation was performed using TransDatRO source code version 1.02, and the ellipsoidal height transformation was performed using the Romanian_ETRS89v102.gsf geoid.

2.6. Reference Data for Accuracy Assessment of Pléiades DTM and DSM Point Clouds

2.6.1. Leveling Measurements

In order to have the most accurate reference for elevations when processing the Pléiades images, leveling measurements were performed based on 14 leveling points from the geospatial control network, using the method of stadia leveling and a Leica Sprinter 100 M electronic level instrument, with a standard deviation for height measurement per 1 km double run of 2 mm. The leveling instrument was placed in the middle of the distance between the leveling point and the new point, whose normal height is to be found. The new points were chosen in open areas, in places where in a radius of at least 1 m the variation of normal height is not significant taking into account the planimetric orientation error of Pléiades images, and also to be identifiable on images, representing road markings (Figure 11a–c) or pedestrian crossings (Figure 11c). For the new points, GNSS-RTK measurements have been performed so that we can interpolate the new point in the Pléiades point cloud and also evaluate the accuracy of the GNSS-RTK elevation value (Figure 11d).
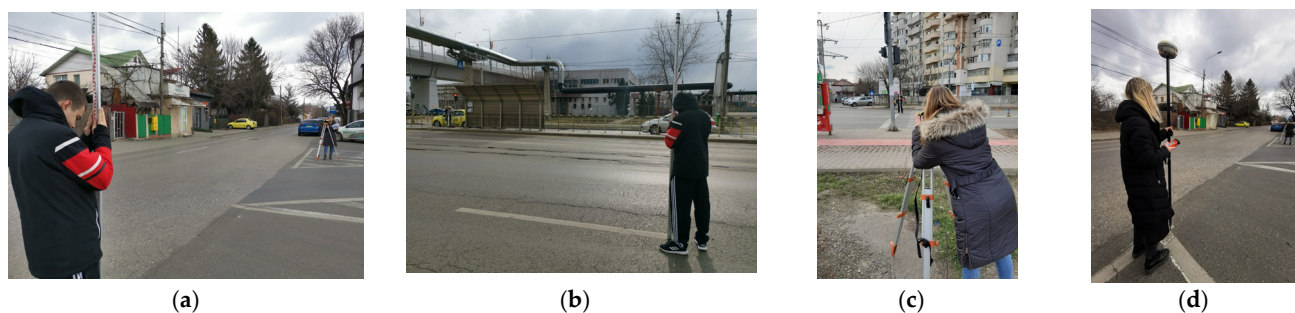

(a)   (b)   (c)   (d)

Figure 11. Example of GNSS-RTK and leveling measurements: (**a**,**b**) leveling measurement of a new point representing road marking; (**c**) leveling measurement of a new point representing pedestrian crossing; (**d**) GNSS-RTK measurement of a new point representing road marking.

Because 17 years elapsed between the execution of the geospatial control network (2005) and the leveling measurements (2022), many leveling points were lost due to processes such as sidewalks modernization (pavements). In consequence, 11 leveling points are in a range area of 1 to 3 km from the Iasi permanent station, and 3 of them are in a range area of 5 to 7.6 km. A total of 18 measurements were performed with an average of 10 GNSS satellites and the precision within the following ranges:

- Position dilution of precision (PDOP) 1.19 ÷ 2.69 (<3), mean PDOP = 1.59,
- Horizontal dilution of precision (HDOP) 0.69 ÷ 1.77 (<2), mean HDOP = 0.86,
- Vertical dilution of precision (VDOP) 0.88 ÷ 2.02 (<3), mean VDOP = 1.34.

Comparing the elevation values resulting from GNSS-RTK measurements with the leveling measurements, an RMSE of 9.1 cm was obtained. For most of the points situated at distances less than 3 km, the differences between RTK-GNSS measurements and leveling measurements are 1 mm ÷ 2 cm. Nevertheless, it is not universally applicable since an error of 4.8 cm was obtained for a point situated at 1 km from Iasi permanent station, an error of 9.3 cm was obtained for a point at 2.2 km from the Iasi permanent station and errors of around 19 cm were obtained for two points situated at 3 km, being measured close to high buildings. In addition, for the three points measured at longer distances from the Iasi permanent station, 5 km to 7.6 km, the errors range from 10 cm to 24.2 cm.

In [36], an investigation on height differences measured by 2 h, 1 h, and 20 min static and RTK surveys was performed by comparing the resulting heights with those measured

by spirit leveling for 20 points. The conclusion of this study was that GNSS static 2 h surveys can provide an accuracy of 3 cm when about 20 GNSS satellites are tracked and that RTK surveys can provide an accuracy of 7 cm when an average of 11 GNSS satellites are tracked, the distances between the rover and the base being less than 1 km. Therefore, our findings are in accordance with this study having performed the GNSS-RTK measurements with approximately the same number of GNSS satellites.

2.6.2. HR ALS Point Cloud

The ALS flight for this dataset was performed at the same time as the previous described flight with the same sensor and wavelength for an area of about 500 km^2 covered by 200 strips. With an acquisition speed of 51 m/s at a flight height of 1200 m and a field of view (FOV) of 27°, a strip width of 580 m was obtained. The planimetric coordinates were calculated in the National Projection System of Romania, namely "Stereographic on a unique secant plane-1970" (STEREO-70), and the normal heights (H) were calculated in the national reference system for heights "Black Sea-1975". The reference dataset covers an area of 1.5 km^2 comprising a total of 4,695,424 points, classified in 7 classes, namely unclassified (class 1), ground (class 2), low vegetation (class 3), medium vegetation (class 4), high vegetation (class 5), buildings (class 6) and low point (noise) (class 7) (Figure 12); the elevations range is 34.02 m ÷ 97.40 m.
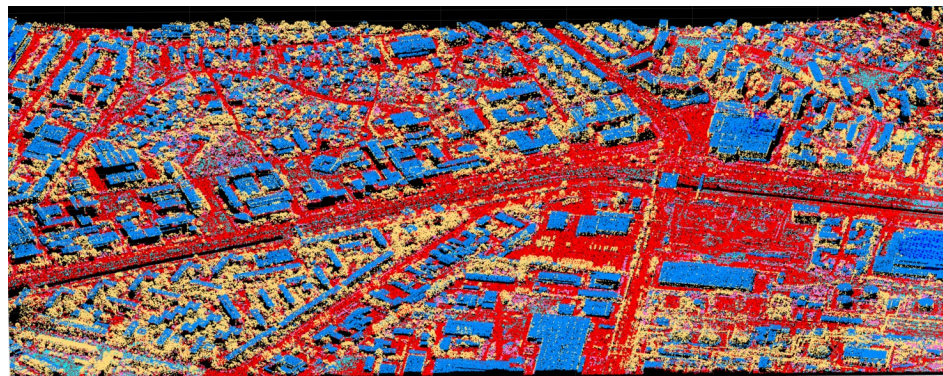

Figure 12. Classified HR ALS point cloud for the study area with a density of 3.1 points/sqm.

3. Data Processing

3.1. Creating the Local Quasigeoid Model

The algorithm that generates the surface for correcting the gravimetric quasigeoid EGG2008 for the study area is based on the combined analytical and geometric methods following the steps described in Figure 13 [47].
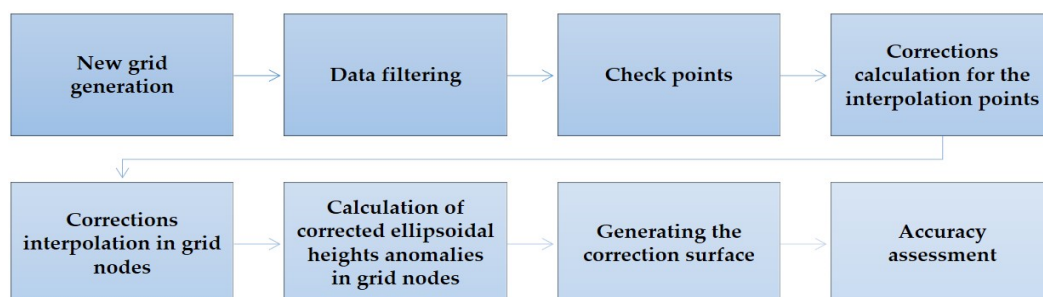

Figure 13. Workflow diagram for generating the surface for correcting the EGG2008 gravimetric quasigeoid.

In the first stage, a new grid was generated in the Surfer_23 software [48] by the bilinear interpolation method, having the same extension as the original one, but with a step of 0°.003 on latitude and 0°.002 on longitude, which corresponds to a grid of 74 × 71 nodes.

By densifying the original grid, a maximum distance of approximately 200 m is kept within each cell, which is intended to prevent significant variation in ellipsoidal height anomalies [49]. Within the data filtering stage, the selection of points with GNSS/leveling measurements was taken into account, for which the differences in absolute value between the calculated ellipsoidal height anomalies ($\zeta_{GNSS/leveling}$) and those interpolated in the new grid (ζ_{EGG}) have residual errors of less than 1.96σ (corresponding to a 95% confidence level). Thus, 50 points were selected to be included in the model for generating the correction surface, and 13 points were extracted to be used for the accuracy assessment of the created surface (Figure 14).
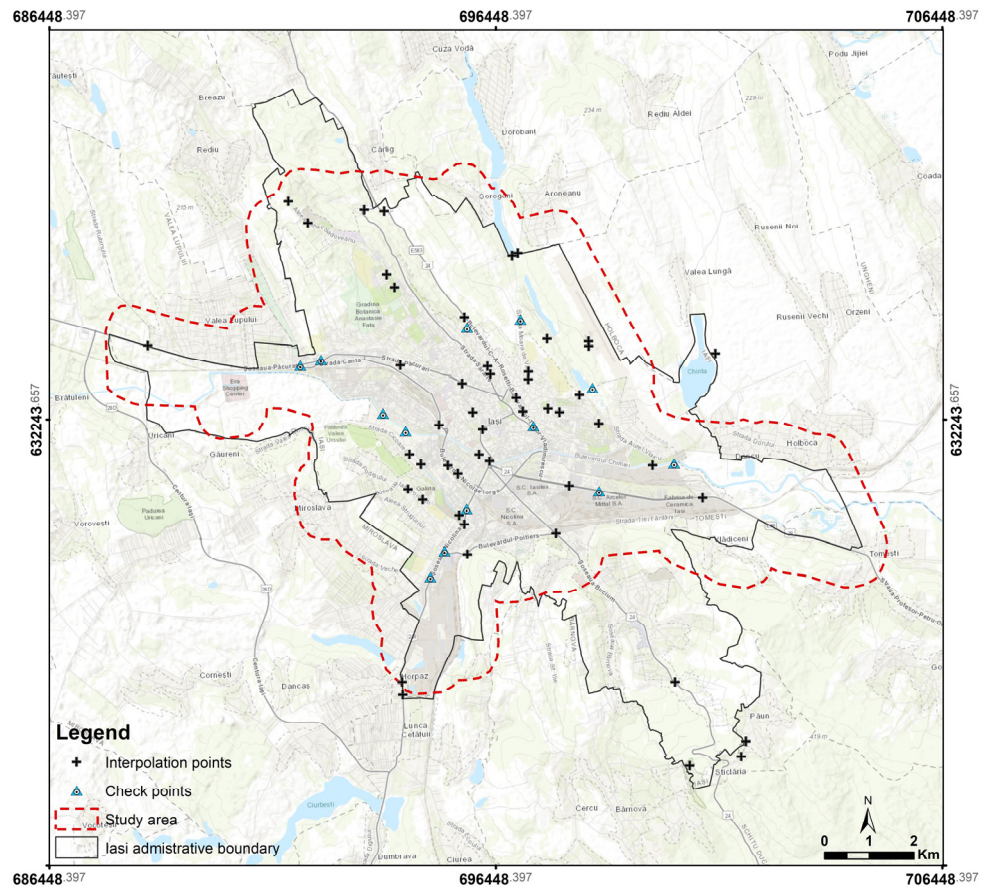

Figure 14. Distribution of the 50 interpolation points and the 13 check points in Iasi city area.

The analytical method involves the calculation of the corrections (V) for the 50 interpolation points, which results from solving the system of correction equations by the least squares method:

$$AX - L = V, \tag{1}$$

where A represents the design matrix, X represents the vector of the unknowns and L represents the vector of the free terms, obtained through the difference: $\zeta_{GNSS/leveling} - \zeta_{EGG}$.

For the case study, the construction of matrix A was chosen based on the basic model with 4 unknown parameters, considering that the application of a complex model with 5 or 7 parameters will not significantly improve the results [46]:

$$A = \begin{bmatrix} \cdots\cdots\cdots\cdots\cdots\cdots\cdots\cdots\cdots\cdots\cdots\cdots\cdots \\ 1° \cos B_i \cos L_i° \cos B_i \sin L_i° \sin B_i \\ \cdots\cdots\cdots\cdots\cdots\cdots\cdots\cdots\cdots\cdots\cdots\cdots\cdots \end{bmatrix}, \tag{2}$$

where B_i and L_i are the geodetic latitude and longitude of the GNSS/leveling point (*i*).

By solving the system and obtaining the vector of unknown parameters

$$X = (A^T A)^{-1} A^T\, L, \tag{3}$$

the vector of corrections (V) can be calculated and then interpolated in all nodes of the grid.

In addition, several interpolation methods available in the Surfer software were tested for defining the most appropriate method for generating the correcting surface. The determination of the corrected ellipsoidal height anomalies (ζ'_{EGG}) in each grid node combines the analytical method by means of the parameters calculated by the rigorous method (X) with the geometric one by means of the interpolated corrections (V′):

$$\zeta'_{EGG} = \zeta_{EGG} + A_i X - V'_i, \tag{4}$$

where matrix A is similarly obtained for the 5254 nodes of the grid.

Finally, based on the new corrected grid, the correcting surface of the quasigeoid is generated and the model accuracy is assessed based on the 13 check points, where the differences have been calculated between the anomalies extracted automatically in the Surfer software (ζ'_{EGG}) and those resulting from measurements ($\zeta_{GNSS/levelling}$).

3.2. LR ALS-DTM Derivation

3.2.1. LR ALS Point Cloud Filtering

The LR ALS-DSM of the study area was created by interpolating all points using the "robust moving plane" interpolation method, implemented into "Grid" module from Opals software [50]. The LR ALS-DSM resulted in a regular grid structure, with a grid cell dimension of 5 m; for each grid cell, the height was estimated by finding the best-fitting tilted plane of the 20 nearest points of the grid point (x,y) found in the 20 m search radius, a detail being presented in Figure 15a. Information gaps remained (void pixels) for the areas covering the lakes around the Iasi city, as no points have been measured. The density of the LR ALS point cloud is not suitable for creating accurate building 3D models, but for DTM derivation the density is acceptable.

(a)   (b)
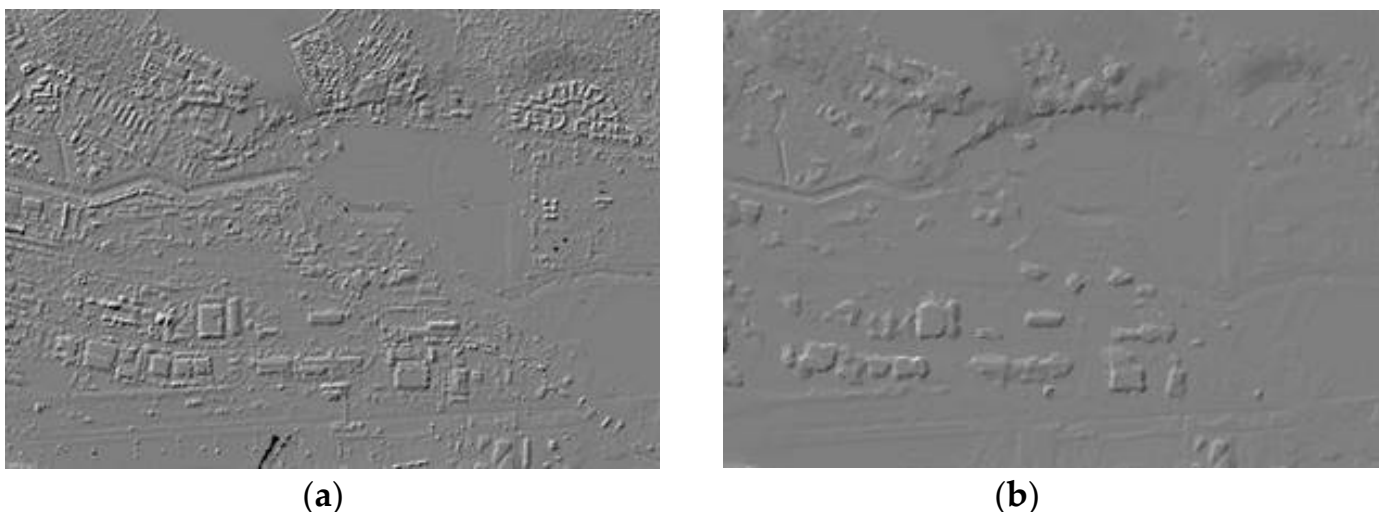
Figure 15. (**a**) Detail of the study area LR ALS-DTM in raster format using moving plane interpolation method (5 m cell size, 20 m search radius, 20 neighbors); (**b**) filtered LR ALS-DTM using the robust filtering method.

To filter the LR ALS point cloud in order to automatically classify the ground and off-ground points, the point clouds corresponding to individual strips have been filtered using the robust filtering method [51] implemented into Opals software with 7 iterations, establishing threshold strips for elevation for noise filtering. The obtained ground points

have been interpolated using the above-described method with the same parameters, the result being a preliminary LR ALS-DTM with a 5 m grid cell for the study area (Figure 15b).

The result is not optimal since there are points on the building roofs that were not filtered, especially for buildings with large footprints, i.e., 20 m, as can be seen in Figure 15b. First, the cloth simulation filter (CSF) [52] implemented in CloudCompare software was tested with the following parameters: the "relief" option for terrain, 5 m for the cloth resolution and 0.5 m threshold for ground point separation. All buildings have been filtered but are together with ground points from forest areas and hilly terrain. The best result was obtained by using the building sub-footprints to filter the buildings' corresponding points. For Iasi city, the building sub-footprints were obtained by stereo-restitution based on ADS-40 aerial flight made in May 2006 at the relative height of 1500 m, covering all the Iasi city area within the project of the urban cadastral survey in Iasi city (Figure 16).

(**a**)   (**b**)

Figure 16. (**a**) Building sub-footprints obtained by stereo-restitution based on ADS-40 aerial images; (**b**) detail.

The step of filtering all ALS points inside the polygons representing the building sub-footprints was completed by creating a buffer of 1 m around the buildings with surfaces larger than 100 sqm in ArcGIS Pro software.

3.2.2. LR ALS-DTM Generation

The LR ALS-DTM was created by combining two raster datasets using the "Algebra" module from Opals 2.3.2 software: the DTM obtained by applying the "robust moving planes" with the same parameters as in the case of the LR ALS-DSM and the DTM obtained by applying the "Delaunay triangulation" interpolation method. For the last raster, the "FillGaps" module was also used to fill the 111 detected gaps (i.e., void pixels) by the triangulation method that calculates the new values by triangulating the boundary pixels of the gap. The final LR ALS-DTM of the study area can be seen in Figure 17.

The LR ALS-DTM heights are ellipsoidal and have been corrected using the correction surface of the local quasigeoid. Thus, the Black Sea-1975 normal heights were obtained by subtracting the anomalies from the ellipsoidal heights using the Opals "Algebra" module. As a final step, a transformation was performed using the ArcGIS software to bring the results into the national coordinate system (STEREO-70) and reference system for heights. The LR ALS-DTM height accuracy was checked against 62 leveling points yielding an RMSE of 39.4 cm and against the 142 GNSS-RTK points yielding an RMSE of 30.2 cm.
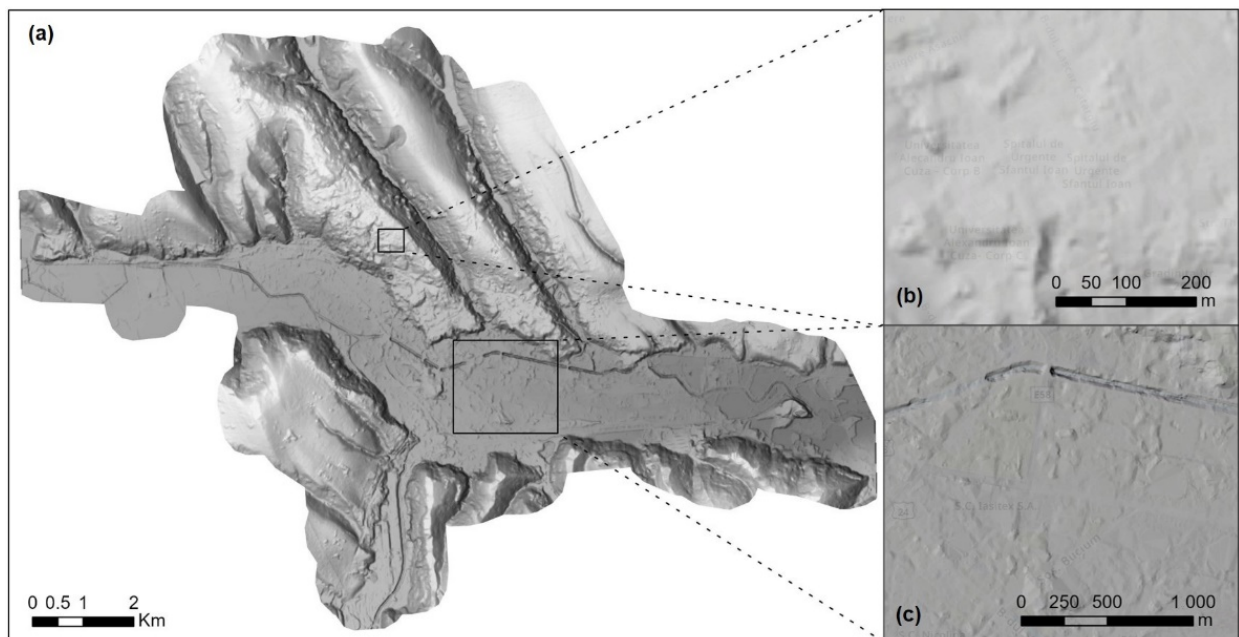
Figure 17. (**a**) Shaded LR ALS-DTM over the Iasi city; (**b**,**c**) detail view in the city areas.

3.3. Pléiades Satellite Image Photogrammetric Processing

The photogrammetric processing of the Pléiades satellite images was performed using the Inpho 8.0 Software from Trimble [53] with the following steps: image measurements of all GCPs and ChPs, RPC refinement with measured GCPs and automatic extraction of tie points (TPs), accuracy assessment of the georeferencing process based on GCPs and ChPs, 3D point cloud reconstruction using dense image matching technique and Pléiades-DSM vertical accuracy evaluation. As mentioned before, for Pléiades image processing, two scenarios were tested: (1) with GNSS-RTK coordinates for all GCPs and ChPs transformed into the national coordinate system for planimetry and heights through the TransDatRO software, without introducing the LR ALS-DTM in the dense image matching process and (2) with the ellipsoidal heights for all GCPs and ChPs corrected with the local quasigeoid and introducing the LR ALS-DTM in the dense image matching process. Specifically, the available elevation information from the LR ALS-DTM is imported in the software and is being used as a prediction parameter in the dense image matching process. The differences between measured and corrected normal heights are in range of -27.6 cm $\div 23.0$ cm, with the standard deviation of 14.1 cm and the RMSE of 15.4 cm.

3.3.1. Image Orientation

The initial satellite image orientation based on the provided RPCs leads to large systematic geoposition biases in object space. Therefore, for improving the image georeferencing by refining the initial values of the RPCs, control points with known coordinates were used. This step was performed by using the Match-AT module of the Trimble Inpho software. The image coordinates of all known points were measured within the software multi-aerial viewer, and their role in the georeferencing process was established by changing the type (HV for GCP and CHV for ChP). From a total of 142 points, 64 served as GCPs and 78 served as ChPs (Figure 18a). TPs were extracted by means of feature-based matching using Förstner operator and refined with least squares matching [11]. TPs with residuals larger than 1 px were removed and the remaining TPs with residuals larger than 0.5 px were remeasured in both images, and approximately 457 TPs were manually recorrected, resulting in a total of 1258 TPs (Figure 18b). The RPC refinement was again performed, and the final standard deviation for image residuals was 0.61 px. As a final step, the accuracy of satellite image orientation was assessed by using the 78 ChPs.
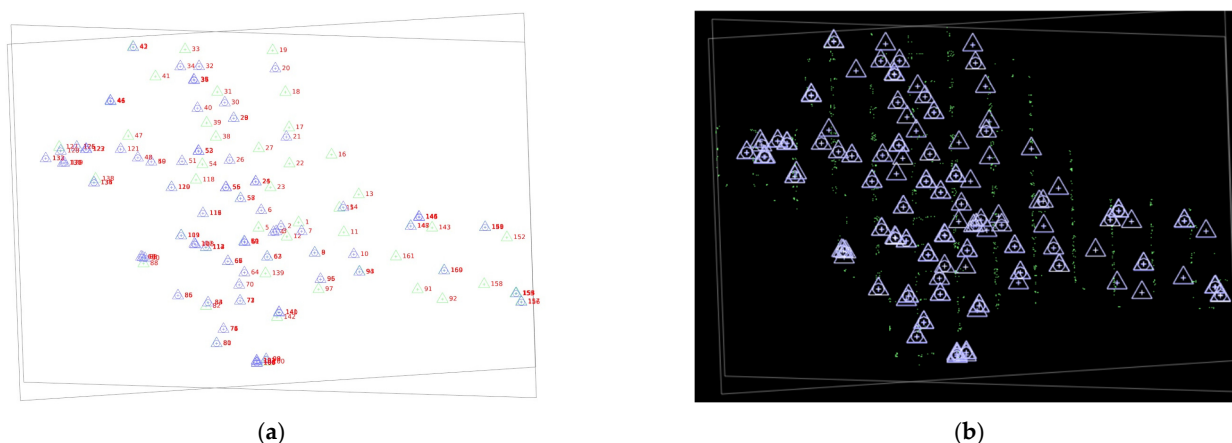
(**a**)   (**b**)

Figure 18. (**a**) Distribution of GCPs (blue color) and ChPs (green color); (**b**) TPs (green) automatically extracted from GCPs and ChPs.

3.3.2. Satellite Image Matching and 3D Reconstruction

The image matching and 3D reconstruction processes were performed using the Match-T DSM module from Trimble Inpho 8.0 Software. This uses three matching strategies: least squares matching (LSM), feature-based matching (FBM) [54] and cost-based matching (CBM). For this case study, from the parameter setting dialog, the type FBM/CBM was selected to perform the dense image matching process for the two panchromatic Pléiades images, previously radiometrically corrected. While the FBM is an area-based matching technique, CBM is a pixel-by-pixel matching technique, where the pixel correspondence is searched through a path in a so-called 3D cost cube [11]. Starting from a coarse approximation to the final accurate result, the software works on image pyramid levels, following an iterative process with 10 steps. To generate a highly dense 3D point cloud, the last 3 pyramid levels are processed with the CBM pixel-wise strategy [11]. For the terrain type, four different options are available: flat, undulating, mountainous and extreme. The grid size is different for each type, starting with a coarser grid size for the flat type ($30 \times$ GSD) and ending with a denser grid size for the extreme terrain type ($21 \times$ GSD) [11]. The "undulating" type was selected for Iasi city area and the resulting 3D photogrammetric point cloud density was set to "dense", i.e., 1 point/pixel, resulting in a long processing type, i.e., 12 h 46′ 11″, using four cores of a 3.50 GHz machine with 32 GB RAM. The results with more than 9 million points are split automatically by the software into multiple tiles, resulting in a number of 150 files.

3.3.3. Pléiades-DTM Generation

Following a similar workflow, point clouds describing only the ground surface (filtered vegetation, buildings, etc.) were also generated by using the Match-T module of the Trimble Inpho 8.0 software, but with the following parameter settings: digital terrain model (generation type), undulating (terrain type), medium (smoothing), medium (feature density), 1 pixel (point cloud density). The smoothing parameter is used to filter the resulting point cloud: higher smoothing factors will lead to less dense point clouds and vice versa. To create a smooth Pléiades-DTM with less detailed surface description and not including small details, such as single trees, a medium smoothing factor was selected. The feature density parameter regulates the number of feature points by defining the number of pixel rows to be used in the automatic extraction. The selected medium feature density uses every second row, resulting in a more generalized Pléiades-DTM surface. The parameter point cloud density defines the number of pixel rows and columns to be used in the automatic extraction of 3D points, with 1 pixel meaning that for each pixel a corresponding 3D point will be extracted [11]. The resulting point clouds with more than 9 million 3D terrain points were derived using the same computer configuration in a shorter time interval of approximatively 38′.

4. Results and Discussion

4.1. The Local Quasigeoid

A first statistical analysis of the data processed by the least squares method refers to the free terms and the correction (v_i) string characteristics ($l_i = \zeta_{GNSS/leveling} - \zeta_{EGG}$) obtained by adjusting 50 interpolation points (Table 2).

Table 2. Statistical analysis of the dataset for differences (l_i) and corrections (v_i).

Data	Arithmetic Mean (m)	Minimum (m)	Maximum (m)	Median (m)	σ (m)
l_i	-0.56 ± 0.02	-0.80	-0.25	-0.59	± 0.14
v_i	0.00 ± 0.02	-0.31	0.21	0.04	± 0.14

An important stage in the generation of the quasigeoid correction surface is the evaluation of several interpolation methods in order to transfer the analytically calculated corrections in the EGG grid nodes. For this, some of the available interpolation methods in the Surfer software were selected [48], for which a series of significant statistical data from the analysis report were extracted. Starting from each interpolation method used to calculate the corrections in the grid nodes, a correction surface of the quasigeoid was generated, which is the basis for determining the accuracy of the model based on the 13 check points. Analyzing the statistical reports of the differences ($\Delta\zeta$) calculated for the interpolation and check points, the smallest differences ($\Delta\zeta$) were obtained for the "Moving Average" interpolation method. Computing the same differences for the official ellipsoidal height transformation model (TransDatRO) by means of the quasigeometric EGG97 correction, the following values were obtained: $\mu = 12$ cm; $\sigma = \pm 24$ cm for the 50 interpolation points and $\mu = 14$ cm; $\sigma = \pm 13$ cm for the 13 check points.

Finally, by comparing the differences obtained for the interpolation and check points using the official ellipsoidal height transformation model with the results obtained for the new interpolated model, a significant improvement in the accuracy brought by the proposed correction surface model can be observed. Thus, the σ calculated for the check points is 4 cm for the newly generated local quasigeoid model in comparison with 13 cm for the official transformation model. The differences between the existing grid included in the official TransDatRO software and the new one generated by the "Moving Average" interpolation method are shown in Figure 19, ranging from 0.30 m to -0.28 m.

4.2. Stereo Pléiades Satellite Image Processing

To study the impact of including an external reference LR ALS-DTM in the dense image matching process of the stereo Pléiades images, we considered two different scenarios: (1) satellite image orientation with no correction applied on GCP ellipsoidal heights and (2) satellite image orientation with GCP ellipsoidal heights corrected based on the local quasigeoid and LR ALS-DTM as additional ground surface information for dense image matching process. Explicitly, in the "Parameter Settings" window "Advanced" tab configuration for the dense image matching process, the LR ALS-DTM was considered as the initial height model. Used as predefined surface information, the LR ALS-DTM was imported in the SCOP (*.dtm) file format.

To ensure a fair comparison, the image measurement coordinates for GCPs and ChPs in scenario (2) are the same as those in scenario (1), having only the elevation changed with the corrected values.

To evaluate the Pléiades image orientation process, three statistical measures were calculated: mean (μ), standard deviation (σ) and the root mean square error (RMSE) values for the differences between adjusted and original coordinates of GCPs and ChPs. The results are presented in Table 3 for the two considered scenarios. Knowing that the ground sample distance (GSD) of the forward panchromatic images is 46 cm and of the backward

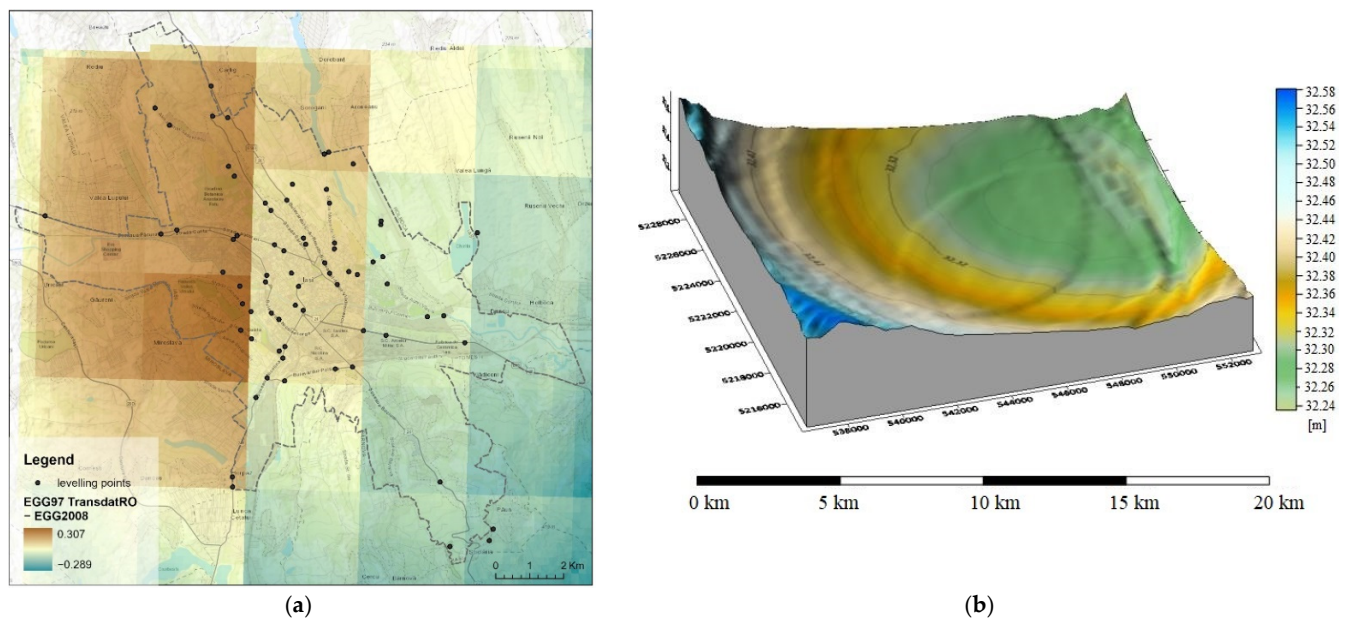image is 51 cm, the errors are also expressed in pixels, with respect to a mean GSD of 49 cm (Table 3).

Figure 19. (**a**) The ellipsoidal height differences between the EGG97 TransDatRO and EGG2008 corrected grid; (**b**) 3D visualization of the correction surface of the EGG2008 grid for Iasi city (WGS84/UTM35N).

Table 3. The residuals of 64 GCPs and 78 ChPs for two scenarios: uncorrected GNSS-RTK measurements and corrected GNSS-RTK measurements with the surface of the local quasigeoid.

No. of GCPs and ChPs		Statistical Values (m/pixels)					
		Not Corrected			**Corrected with Both the Local Quasigeoid and the LR ALS-DTM in the Process of Image Matching**		
		X	Y	Z	X	Y	Z
64 GCPs	μ	0.00/0.00	0.00/0.00	0.00/0.00	0.00/0.00	0.00/0.00	0.00/0.00
	σ	0.13/0.27	0.14/0.29	0.07/0.14	0.14/0.29	0.14/0.29	0.08/0.16
	RMSE	0.13/0.27	0.14/0.29	0.07/0.14	0.13/0.27	0.14/0.29	0.08/0.16
78 ChPs	μ	−0.10/−0.21	0.05/0.11	0.07/0.14	−0.12/0.24	0.05/0.11	0.04/0.08
	σ	0.65/1.32	0.78/1.60	0.71/1.44	0.64/1.31	0.78/1.59	0.71/1.44
	RMSE	0.66/1.34	0.78/1.60	0.70/1.43	0.62/1.26	0.74/1.51	0.67/1.37

Regarding the planimetric errors ($RMSE_{X,Y}$) calculated for GCPs, they are very small, suggesting that the GCP identification in images was better than one-third of a pixel, as also reported in [6]. The vertical errors are 7 cm for the uncorrected scenario and 8 cm for the corrected scenario, representing 0.14 GSD. In contrast with the residuals reported in literature, the obtained error is better, representing half of the error reported in [6] with respect to GSD and a quarter with respect to the metric value. Regarding the planimetric errors ($RMSE_{X,Y}$) calculated for ChPs, they are 1.02 m (2.08 GSD) for the uncorrected scenario and 96 cm (1.96 GSD) for the corrected scenario, the improvement being 6 cm. Regarding the vertical errors, these are 70 cm (1.43 GSD) for the uncorrected scenario and 67 cm (1.37 GSD) for the corrected scenario, comparable with the ones reported in [13] and better than the errors reported in [6] and those reported in [33] for both test sites (Ticino, 1.04 m; Ljubljana, 0.80 m). In addition, the improvement when using the corrected GNSS-RTK measurements and the LR ALS-DTM in the process of image matching is 3 cm in the Z direction when checking against the 78 ChPs.

The dense image matching algorithm was applied individually for each scenario, resulting in dense 3D photogrammetric point clouds in LAS file format, with an overall regular distribution and density of 4 points/m². Their reported vertical quality was assessed against the available GCPs, ChPs and adjusted TP coordinates (Table 4). Compared to scenario (1), when using the corrected GCP ellipsoidal height values with the local quasigeoid surface and additional LR ALS-DTM for dense image matching in scenario (2), the vertical accuracy of GCPs and ChPs is improved by 9 cm.

Table 4. Vertical evaluation of the 3D reconstructed point clouds for the two scenarios: uncorrected GNSS-RTK measurements and corrected GNSS-RTK measurements with the local quasigeoid surface and using the LR ALS-DTM in the dense image matching process.

No. of GCPs, ChPs, TPs	RMSE Values (Z) for the Used Points (m)	
	Not Corrected	Corrected
64 GCPs and 78 ChPs	0.698	0.609
1258 TPs	1.094	1.093

4.3. Evaluation of Pléiades Point Clouds Obtained by Using the Two Scenarios, Corrected and Not Corrected

4.3.1. Qualitative Evaluation of DSM Point Clouds Derived in Two Scenarios: Corrected and Not Corrected

First, the qualitative assessment of the DSMs generated from the Pléiades image data for both scenarios focused on computing the differences between them in the form of $DSM_{Not\ corrected} - DSM_{Corrected}$.

As shown in Figure 20, the values range from -68.09 m to 64.81 m with a standard deviation of 1.045 m and a mean of -0.064 m. The differences mainly occur for the high vegetation areas and also occur on the edges of high buildings situated at close distances from each other with trees placed in between. Moreover, positive and negative biases can be observed on building roofs caused by architectural elements and other features such as chimney roofs, different roof types (e.g., cross gable roof), towers and shadows.
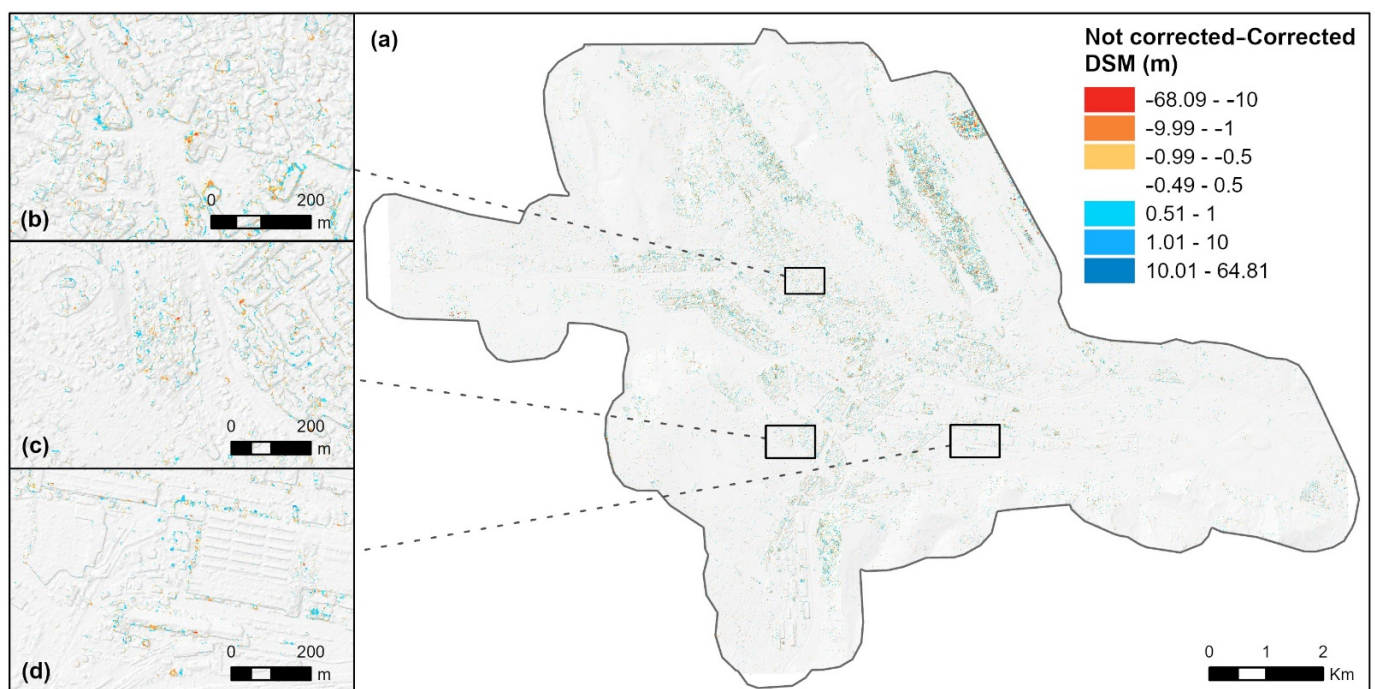

Figure 20. (**a**) Difference raster between the two scenarios for DSM, not corrected and corrected, and detailed view over (**b**) a central part of the city, (**c**) a residential hilly area and (**d**) an industrial site.

Upon visually analyzing the Pléiades-DSM point clouds resulting from the dense image matching process, positive and negative biases were observed for both scenarios, corrected and not corrected. While points below the Pléiades-DTM surface can be observed in certain areas in the uncorrected scenario, these outliers are not present in the corrected scenario. Moreover, in the first scenario (not corrected), points representing picks on the roofs of the buildings with a height between 10 and 30 m will affect the accuracy of the automatic determination of building heights (Figure 21). Figure 22 presents five buildings with their corresponding profiles for a visual comparison between the Pléiades-DSM point clouds resulting from the two scenarios and the HR ALS-DSM (Figure 22). The HR ALS-DSM and Pléiades-DSM point clouds (Figure 22a–c) are classified based on their height for a visual comparison of the building structures.
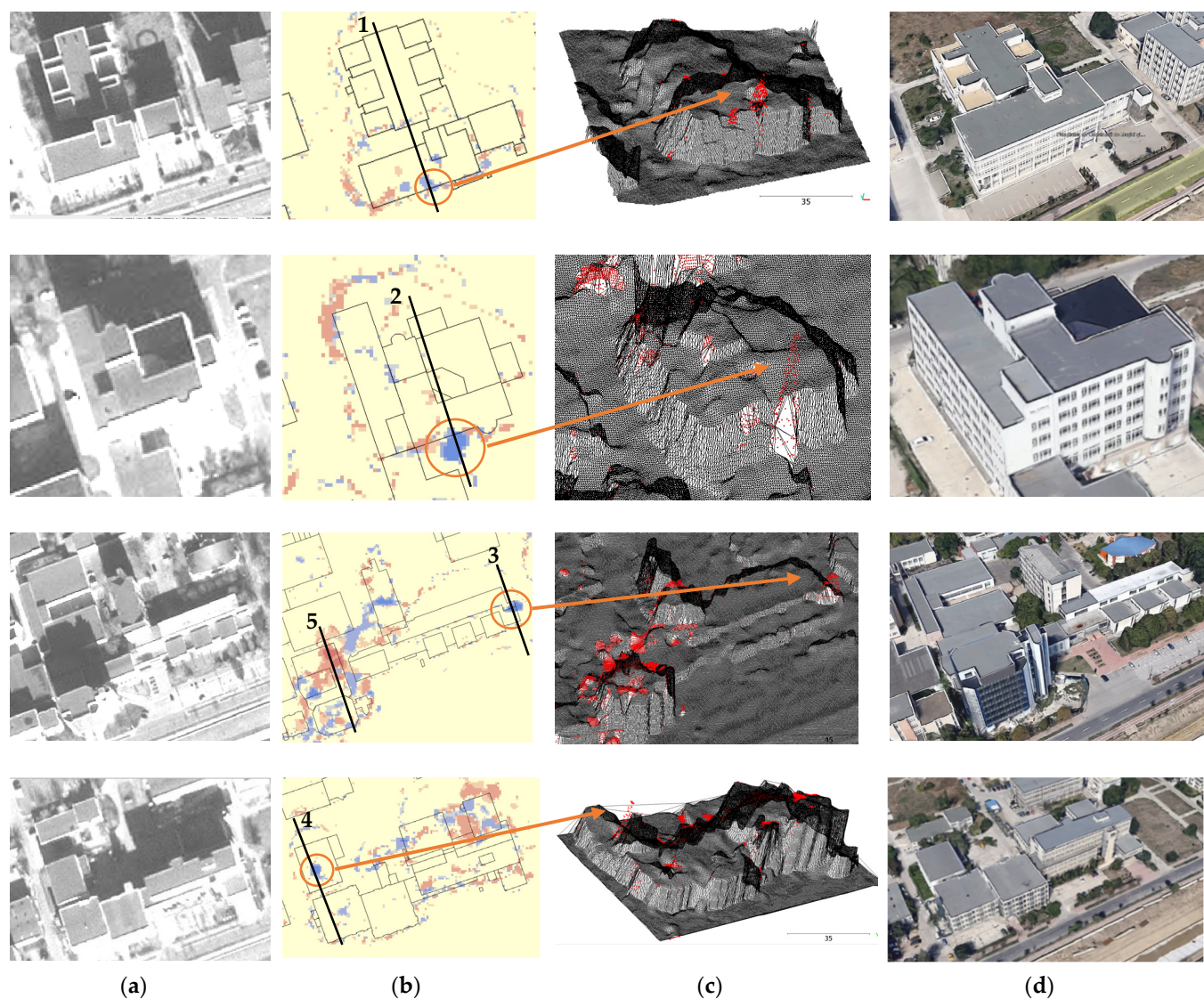

(**a**)   (**b**)   (**c**)   (**d**)

Figure 21. (**a**) Pléiades image detail; (**b**) map of differences between the uncorrected and corrected Pléiades-DSM point clouds and the labeled profile trajectory (black line) (the color legend from Figure 20 is applicable); (**c**) mesh for the corrected Pléiades-DSM and red color uncorrected Pléiades-DSM (orange circles and arrows indicate the positive differences in 3D); (**d**) Google Earth detail.

4.3.2. Quantitative Evaluation of the Pléiades DTM and DSM Point Clouds Derived in Two Scenarios: Corrected and Not Corrected

The Pléiades-DTM point clouds have been evaluated against 62 leveling points from the geospatial control network of Iasi city out of a total of 71 and against 142 GNSS-

RTK in situ measurements in an overall evaluation and by comparison with the HR ALS point cloud.

(**a**)　　　　　　　　　　　　　　(**b**)　　　　　　　　　　　　　　(**c**)

Figure 22. *Cont.*
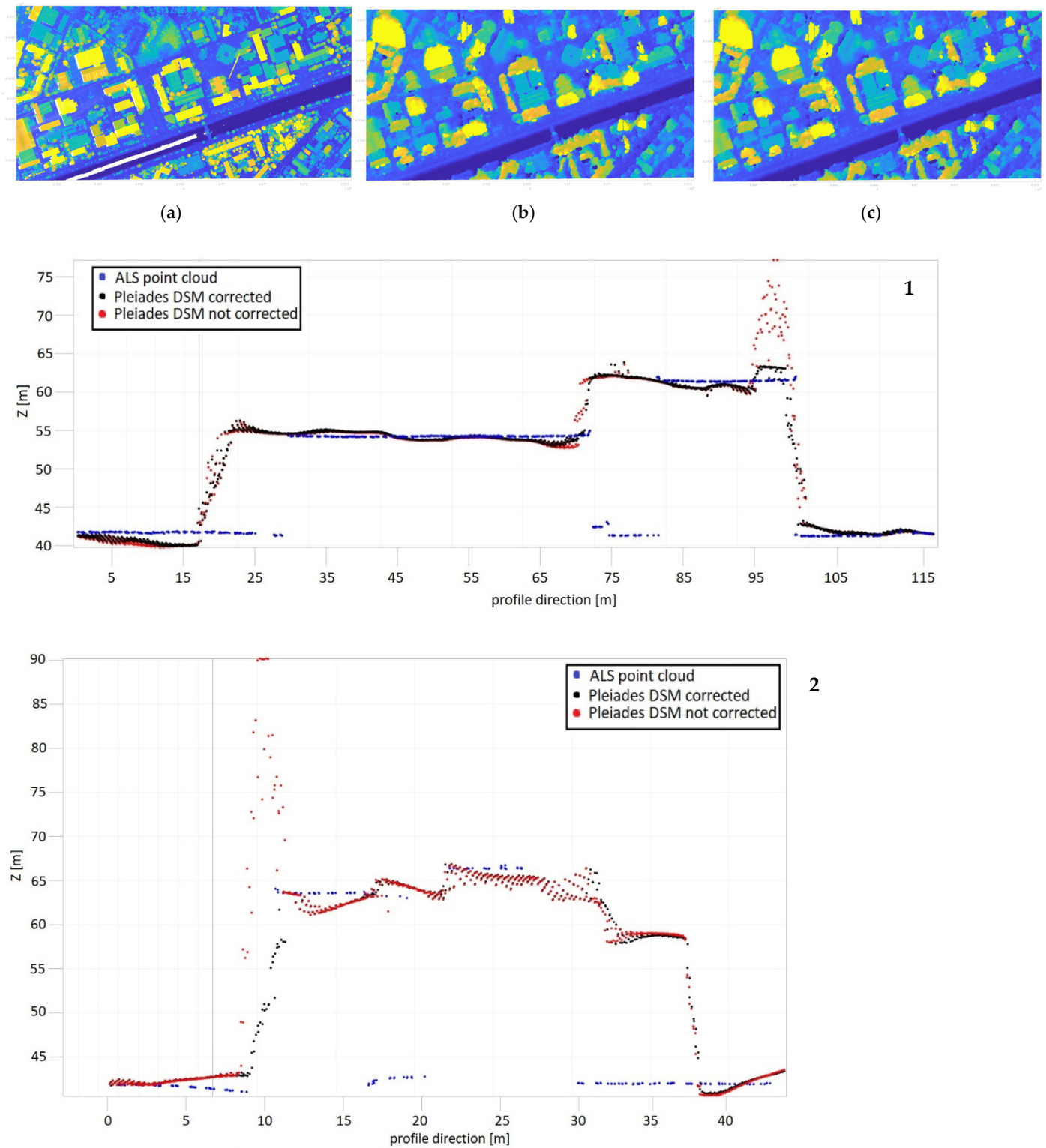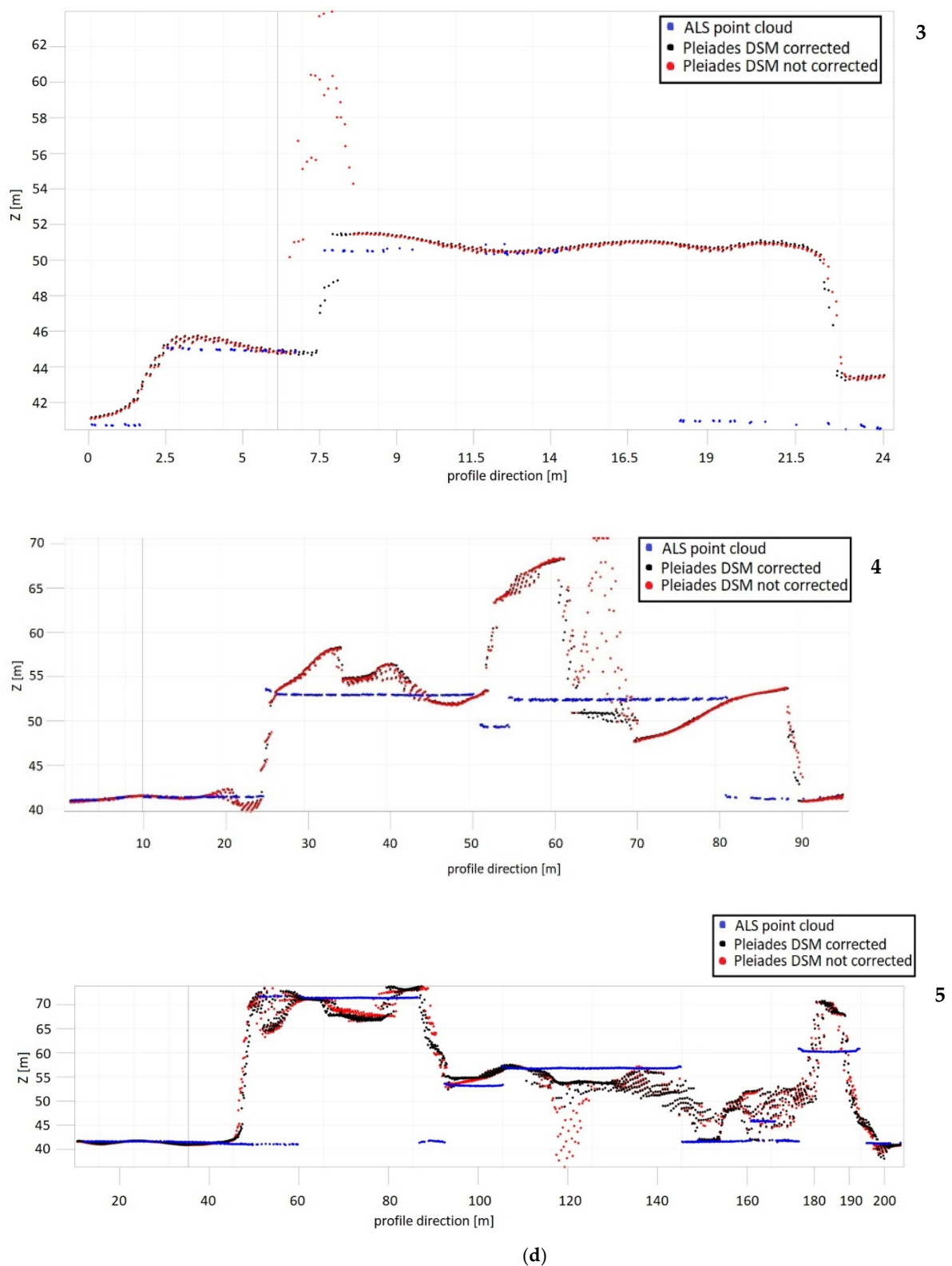
(**d**)

Figure 22. (**a**) HR ALS-DSM point cloud; (**b**) Pléiades-DSM corrected point cloud; (**c**) Pléiades-DSM uncorrected point cloud; (**d**) profile of 2 m width of the Pléiades-DSM point clouds for both corrected and uncorrected scenario pairs in comparison to the reference HR ALS-DSM, for the five analyzed buildings (1–5 labeled profile trajectories highlighted in Figure 21b).

Overall Quantitative Evaluation of the Pléiades DTM and DSM Point Clouds

Using the ArcGIS software, the elevations of the leveling and GNSS-RTK points were interpolated in the Pléiades DTM and DSM point clouds, respectively, derived using the two scenarios. The mean, standard deviation and root mean square error values for the differences between initial elevations and the interpolated ones are summarized in Table 5. We have to mention that five points have been identified as outliers in the case of leveling points and six points have been identified as outliers in the case of GNSS-RTK points; the statistical values were computed without these points.

Table 5. The residuals of the 57 leveling points and 136 GNSS-RTK points for two scenarios: uncorrected GNSS-RTK measurements and corrected GNSS-RTK measurements with the surface of the local quasigeoid and using the LR ALS-DTM in the image matching process (without outliers).

Stereo Pléiades Products		Reference Points (without Outliers)			
		Leveling		GNSS-RTK	
		Corrected (cm)	Not Corrected (cm)	Corrected (cm)	Not Corrected (cm)
DTM	μ	32.7	39.2	39.5	46.1
	σ	83.8	84.4	62.5	64.0
	RMSE	90	93.0	71.3	75.8
DSM	μ	76.1	84.8	31.1	44.6
	σ	121.3	137.1	62.0	64.1
	RMSE	87.3	92.1	66.2	74.6

As mentioned in the introduction part, the comparison between our results and the results obtained from other studies is not fair since most of them used GCPs and CPs measured on the existing orthophoto with the elevations extracted from the corresponding DTM for accuracy assessment, the accuracies of the measured GCP and CP object coordinates being in the order of 20 cm in planimetry and 25 cm in the vertical direction [33]. However, we have put our results in a broad context, concluding that the RMSE value of the Pléiades-DTM point cloud for the corrected scenario of 71.3 cm is smaller than the value reported by [13], i.e., 85 cm for a tri-stereo Pléiades.

Regarding the Pléiades-DSM, the RMSE for the corrected scenario is 66.2 cm, which is improved by 8.4 cm compared to the uncorrected scenario. In addition, the residual is better than the RMSE value reported in [33] for a total of 25 GCPs and CPs and is 79 cm for the first study area and around 70 cm for the second area.

The 18 stadia leveling points have been interpolated in the Pléiades-DSM point clouds, resulting in a σ value of 40.4 cm and an RMSE value of 69.0 cm for the uncorrected scenario, while a σ value of 38.5 cm and an RMSE value of 65.2 cm were obtained for the corrected scenario. An improvement of 3.8 cm was achieved for the corrected scenario, and it should be mentioned that 15 points are situated at distances not exceeding 3 km from the Iasi permanent station.

Quantitative Evaluation of the Pléiades DTM and DSM Point Clouds Using the HR ALS Point Cloud

The HR ALS-DTM with a GSD of 0.5 m was created based on the HR ALS point cloud following the steps described in [7] considering only the ALS ground points. For the quantitative evaluation of the Pléiades-DTM point cloud, the Opals software was used to compute the distances between each Pléiades-DTM point and the HR ALS-DTM raster surface in the form of the "NormalizedZ" attribute [7]. From all statistical measures (min, max, mean, median, StdDev, StdDevMAD, RMS), we will closely analyze the standard deviation and the median absolute deviation (StdDevMAD) which is a robust statistic, resulting in a more resilient data quantification due to the fact that large deviations as

outliers do not have a greater impact on the final result. Analyzing the histogram of the distance distribution, it was noticed that the calculated distances are in the range of -7.39 m $\div$ $+20.98$ m with the σ^{MAD} being ±1.07 m in the case of the corrected scenario and in the range of -7.36 m $\div$ $+22.45$ m with the σ of ±1.09 m for the uncorrected scenario. We have to mention that for the direct output of the Match-T module regarding the Pléiades-DTM point cloud, no editing or filtering has been applied. By introducing the ALS-DTM in the process of dense image matching, the error range is reduced, the maximum error being approximately 1.5 m smaller in the case of a corrected scenario. Taking into account the elevation accuracy of around 1 m, a range interval between -1 m and $+1$ m was chosen, the σ^{MAD} being ±42 cm in the case of the corrected scenario and ±43 cm in the case of the uncorrected scenario.

In the case of Pléiades-DSM point clouds, the same steps were applied as in the case of Pléiades-DTM, and the HR ALS-DSM in raster format was first created as described in [7]. The calculated distances are in the range of -46.08 m $\div$ $+64.67$ m with the σ_{MAD} being ±1.252 m in the case of the corrected scenario and in the range of -53.48 m $\div$ $+67.14$ m with the σ of ±1.253 m for the uncorrected scenario, the maximum error being approximately 2.5 m smaller in the case of corrected scenario. In addition, the residuals were computed for the points that fall in the range of ±1 m, and the σ^{MAD} was approximately 3 times smaller than the values obtained for the unfiltered Pléiades DTM and DSM point clouds, with insignificant differences between corrected and uncorrected scenarios. The percentage of these points is 49% for the Pléiades-DTM and 53.9% for the Pléiades-DSM in the case of the corrected scenario, with a 2% improvement against the uncorrected scenario. The results for the Pléiades DTM and DSM point cloud analysis against ALS-DTM and ALS-DSM, respectively, can be seen in Table 6.

Table 6. Standard deviation and the median absolute deviation obtained for the Pléiades DTM and DSM point clouds in comparison with the HR ALS-DTM and HR ALS-DSM, respectively.

Stereo Pléiades Products		Comparison with HR ALS-DTM and HR ALS-DSM			
		Not Filtered		Filtered (-1 m $\div$ $+1$ m)	
		Corrected (m)	Not Corrected (m)	Corrected (m)	Not Corrected (m)
DTM	σ	2.782	2.833	0.421	0.424
	σ^{MAD}	1.073	1.092	0.420	0.430
DSM	σ	5.078	5.102	0.464	0.465
	σ^{MAD}	1.252	1.253	0.479	0.481

The authors of [33] performed a comparison between the nDSMs derived from tri-stereo and stereo Pléiades images and the reference nDSMs derived from aerial image matching, for two test sites and for open stable and tree-covered areas, obtaining a σ_{MAD} for the forward–backward image pair in Ticino before least square matching of 1.12 m in stable areas and of 2.05 in tree-covered areas, while for the Ljubljana study area (28 July stereo-pair), a σ_{MAD} of 60 cm was obtained for the stable areas and a σ_{MAD} of 3.89 m was obtained for the tree-covered areas. With σ_{MAD} of 1.07 m for the DTM and 1.25 m for the DSM considering a 1.5 km^2 urban area in the present study, our results are better than those reported in [33] and comparable with those reported [13] for the stereo-pairs within the incidence angle of [0, 20] (σ, 4.07 m; normalized median absolute deviation (NMAD), 1.14 m).

In [13], a coarse DTM was introduced in the image matching processing as a prediction parameter, specifically the SRTM model, and it was concluded that if a low-resolution DTM is involved in this stage, it improves the robustness of the entire process. The results of the present study are in accordance with these findings; moreover, the quantitative impact when using a high-resolution DTM is evaluated.

4.4. Three-Dimensional Building Modeling LOD1

Once the Pléiades DTM and DSM point clouds were evaluated, further investigations were conducted to test the potential of Pléiades-DSM point clouds obtained under two scenarios for 3D building modeling with LOD1. An essential part of deriving the 3D LOD1 reconstruction of the buildings is to extract the height of the buildings from the Pléiades DSM point cloud. The height attribute can be obtained from different methods that imply calculating the mean or the median of the roofs to extract the height value of the building centroid [55] or the highest value within the building footprint [56].

In this regard, the results are expressed for a central flat area of 1500 × 1000 m with 1550 university and residential buildings, and the mean and median heights were computed for the points inside the building footprint for the two scenarios. The calculated heights have been compared with the reference height from the HR ALS points cloud, resulting in the residual errors for each building height. Based on these residuals, the standard deviation was calculated, and Table 7 differentiates the cases of considering all buildings in the study area, considering the five highlighted buildings with profiles in Figure 22 and considering only the buildings with heights improved by the proposed methodology.

Table 7. Standard deviation obtained for two methods for deriving building height: mean and median height for the points inside the building footprint.

Building Number	Standard Deviation			
	Mean Height		Median Height	
	Corrected (m)	Not Corrected (m)	Corrected (m)	Not Corrected (m)
All buildings	4.1	4.2	4.1	4.2
5 buildings	2.65	2.8	2.37	3.9
Buildings with heights improved by proposed methodology	4.0	4.15	3.9	3.95

Furthermore, based on the residuals derived for each scenario, the absolute difference between the residuals of the corrected scenario and the uncorrected scenario was extracted. The negative obtained values of the absolute differences represent the building heights improved by the proposed methodology. The positive values were classified in five intervals. Considering 10 cm as a threshold, intervals are 0 m to 0.1 m, 0.1–0.2 m, 0.2–0.3 m, 0.3–1 m and above 1 m. The first positive interval is equivalent to the buildings with the same height values in the threshold limits.

It is noticeable that for all buildings, the standard deviation is improved by 10 cm for the corrected scenario for both methods, mean and median. For the buildings with heights improved by the proposed methodology, the standard deviation is improved by 15 cm for the mean method and 5 cm for the median method. Moreover, when analyzing the five buildings taken into consideration in Figure 22, the standard deviation is improved by 15 cm for the mean method and by 1.53 m for the median method.

For the absolute difference between the mean height and median height residuals of corrected and uncorrected scenarios, histograms were computed based on the six defined ranges (Figure 23) and are displayed in the cartographic materials from Figure 24.

Upon analyzing the histograms and the maps, the results show similar percentages for both methods, mean and median. The proposed methodology improves the computed building height by 56%; for 27%, the height values are the same in the threshold limits, while for the following two intervals ranging between 0.1 m and 0.3 m, the uncorrected scenario gives better results with 8%. In addition, better results have been obtained for the uncorrected scenario for the last two intervals, 0.3–1 m and above 1 m, respectively, but with a percentage smaller than 5%.
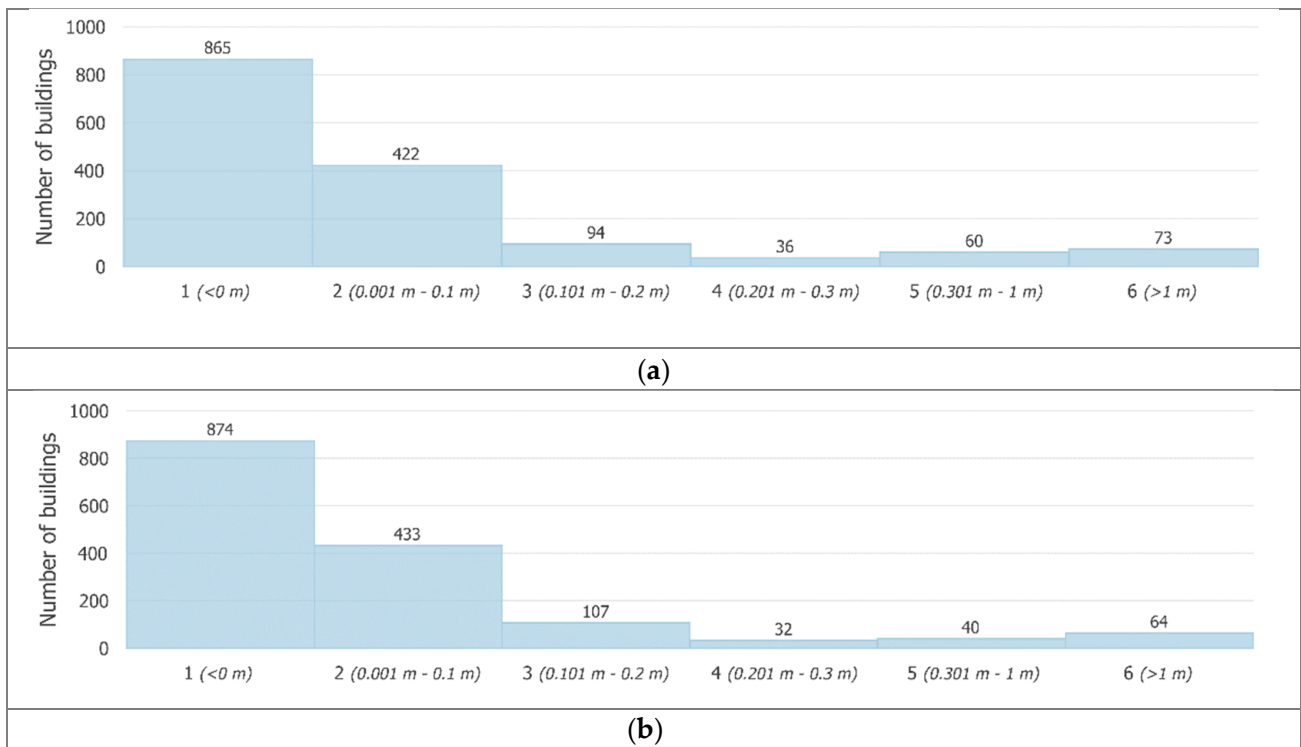
(a)

(b)

Figure 23. The histogram of absolute differences between (**a**) mean height and (**b**) median height residuals for two analyzed scenarios: corrected and not corrected.
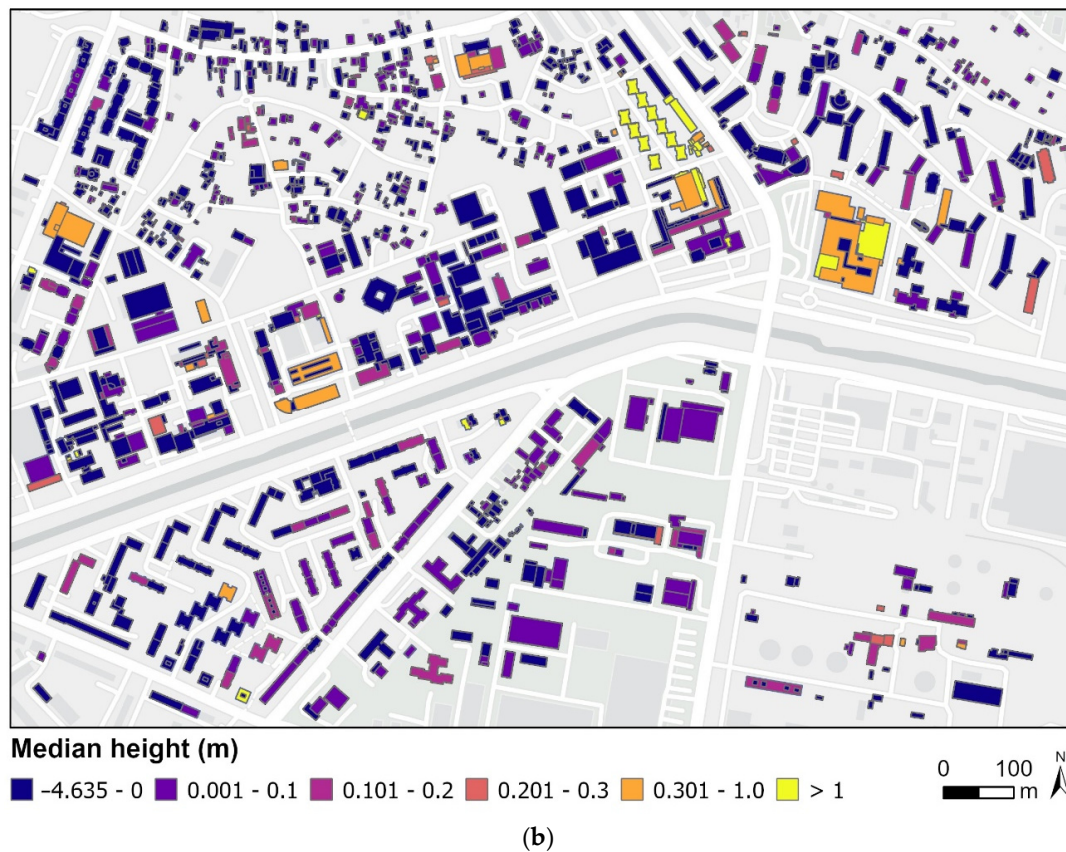

(a)

Figure 24. *Cont.*

Figure 24. Map of building height residuals calculated by mean method (**a**) and median method (**b**).

Further, three approaches were tested for the 1550 buildings. In the first scenario, the height of the centroid was calculated; the second strategy was focused on extracting and averaging the values found in a 1 m buffer around the centroid, while in the third approach, a 1 m interior buffer was applied for the building footprints with the purpose of excluding the points specific to the facades, followed by the computation of the mean and median for all the points found in the shrunken footprints. Figure 25 shows the placement inside a building footprint of the three approaches: centroid, centroid with a 1 m buffer and the 1 m inside buffer for the footprint.
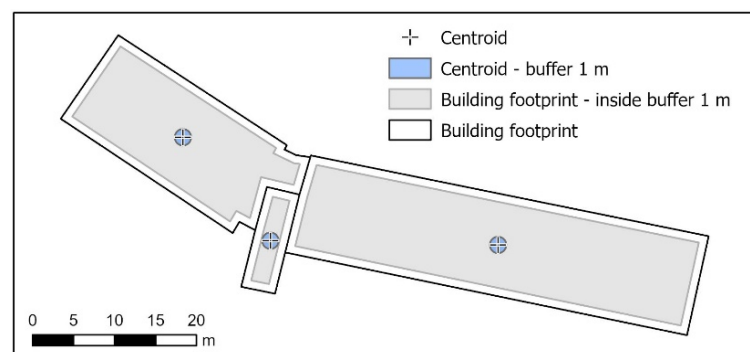

Figure 25. The centroid, the 1 m buffer around the centroid and the 1 m inside buffer for the footprint are visualized for a building.

The results obtained for each approach can be seen in Table 8.

The standard deviation values of the height extracted for the centroid are the highest, 1.7 m for the corrected scenario and 1.82 m for the uncorrected scenario. In contrast, when applying a buffer around the centroid, by averaging the height of the points, the

standard deviation is improved by 6 cm for the uncorrected scenario and 5 cm for the corrected one. Moreover, if the points belonging to the facade are eliminated from the selection by shrinking the building footprint by 1 m, the results range between 1.73 m for the uncorrected scenario and 1.68 for the corrected scenario when the average is calculated. Comparable with the mean height, the standard deviation improves when the median height is calculated, by 6 cm for the uncorrected scenario and by 8 cm for the corrected scenario. From all the tested approaches, the median height calculated for the 1 m inside buffer of the building footprint method performs the best.

Table 8. Standard deviation obtained for the four tested approaches for deriving the building height: centroid, centroid with 1 m buffer and the footprint with an inside buffer of 1 m.

		Standard Deviation (m)					
		Height Value		**Mean Height**		**Median Height**	
		Not Corrected	**Corrected**	**Not Corrected**	**Corrected**	**Not Corrected**	**Corrected**
Centroid	σ	1.82	1.75	-	-	-	-
Centroid buffer 1 m	σ	-	-	1.76	1.70	-	-
Footprint inside buffer 1 m	σ	-	-	1.73	1.68	1.67	1.60

The dash (-) represents that the values were not computed.

Regarding the 3D building reconstruction (Figure 26), the median height of the buildings was associated with the geometry of the sub-footprints available from ADS-40 images and extruded in order to derive the LOD1 3D model. The results obtained for the median height of 1.60 m are better than other studies; [6] had a residual height value of 2.02 m for Pléiades tri-stereo images, and for GeoEye-1, [5] retrieved a residual value of 1.94 m.
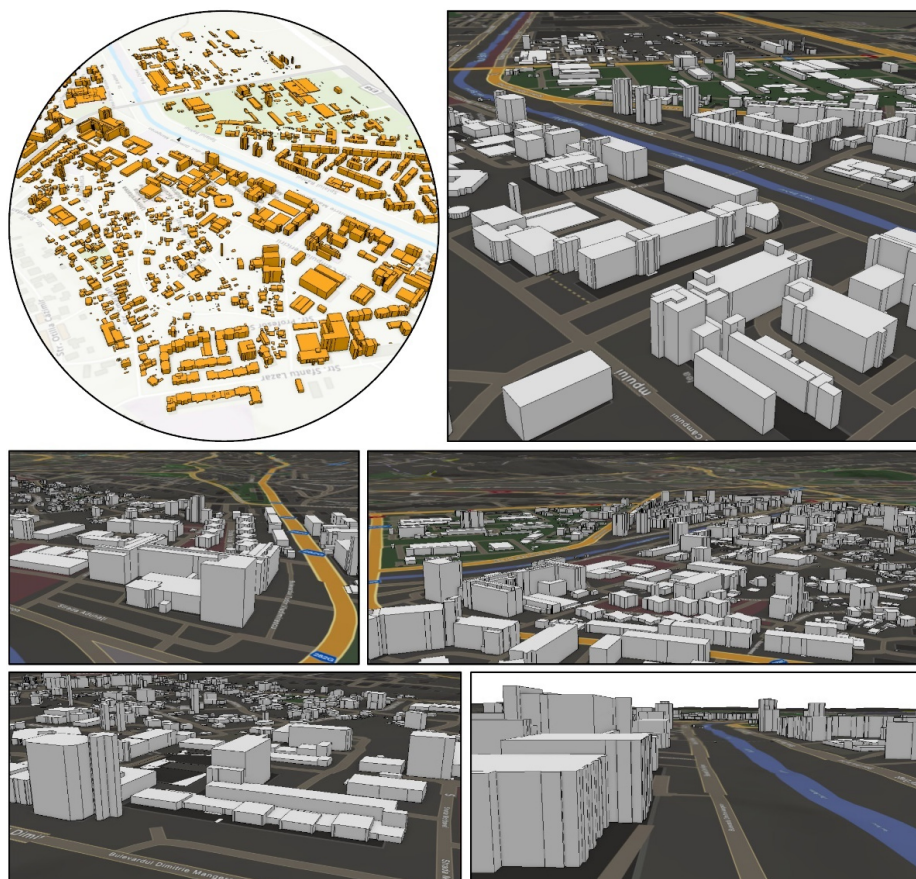

Figure 26. Three-dimensional building reconstruction based on the median height.

5. Conclusions

This study addresses all the steps to obtain a high-accuracy Pléiades-DTM and Pléiades-DSM to reconstruct buildings with LOD1 based on existing building sub-footprints and a single Pléiades stereo-pair of images with an overall convergence angle of 19°, which, being less than 20°, is a small convergence angle according to [13]; the vertical accuracy of DTM and DSM is influenced by the acquisition geometry, the B/H ratio, and the number and coordinate accuracy of GCPs.

Three-dimensional models of topography, especially 3D city models, are often used together with other data sources (i.e., ADS-40-derived building footprints). Therefore, it is of high importance that these datasets have the same datum and are in the same projection. The transformation from GNSS ellipsoidal heights into local systems, including a projection, can be performed with various approaches, which have different levels of rigorousness and feasibility.

To improve the absolute geolocation of the stereo Pléiades image final products, this paper covered all necessary steps, from carefully selecting the GCPs on images (to be situated in areas that did not suffer changes between the year of image acquisition and the year of GNSS-RTK measurements and to be visible on the images), field measurements for all points (142 GCPs and ChPs), performing leveling measurements to test the GNSS-RTK normal height accuracy and finally correcting the ellipsoidal heights with the local quasi-geoid. With a medium number of 12 tracked satellites for the GNSS-RTK measurements and the fact that some points are located in obstructed areas, the elevation accuracy is not optimal, and it is necessary to apply corrections based on the local quasigeoid, the standard deviation of the differences between measured and corrected elevations being 14.1 cm. The accuracy assessment was performed for two different scenarios: (1) no DTM and GCPs and ChPs with uncorrected ellipsoidal heights (uncorrected scenario) and (2) with LR ALS-DTM and GCPs and ChPs with corrected ellipsoidal heights (corrected scenario). The corrected scenario performed the best in all the workflow stages, even if by just a few centimeters in most of the analyzed cases. As such, when evaluating the vertical accuracy of the Pléiades-DTM, an RMSE of 90 cm was obtained against 57 leveling points, an RMSE of 71.3 was obtained against 136 GNSS-RTK points and a σ^{MAD} of 1.07 m was obtained against HR ALS-DTM. Evaluating the vertical accuracy of the Pléiades-DSM, an RMSE of 87.3 cm was obtained against 57 leveling points, an RMSE of 66.2 cm was obtained against 136 GNSS-RTK points and a σ^{MAD} of 1.25 m was obtained against HR ALS-DSM. The accuracy of the building heights for reconstructing the buildings in 3D with LOD1 is the best reported in the literature i.e., 1.6 m, even when compared with GeoEye-1. When calculating building height with the proposed method, the positive biases observed in the Pléiades-DSM uncorrected point cloud have small influences on height extraction, the improvement being up to 7 cm when the corrected scenario is used.

As also shown by Perko et al. [13], introducing previously available surface elevation information in the image matching process as a prediction parameter improves the robustness of the entire process, considerably reducing the systematic effects. This is also reflected by our current study where we further evaluated the quantitative impact of the LR ALS-DTM on the final products. Our main findings can contribute to a high-quality 3D urban reconstruction from satellite stereo imagery and can be very useful for retrieving accurate information from other spaceborne stereo platforms.

Author Contributions: Conceptualization, V.-E.O., A.-I.B., C.C., A.-M.L. and N.P.; data curation, V.-E.O., A.-I.B., C.C., A.-M.L., M.M. and A.-M.N.P.; formal analysis, A.-I.B., V.-E.O., C.C., A.-M.L. and N.P.; funding acquisition, V.-E.O. and A.-M.N.P.; investigation, A.-I.B., V.-E.O. and N.P.; methodology, V.-E.O., A.-I.B., C.C., A.-M.L. and N.P.; project administration, A.-I.B. and V.-E.O.; resources, A.-I.B. and V.-E.O.; software, A.-I.B., V.-E.O., C.C. and A.-M.L.; supervision, V.-E.O., A.-I.B. and N.P.; validation, V.-E.O., A.-I.B., C.C., A.-M.L. and N.P.; visualization, A.-I.B., V.-E.O., C.C., A.-M.L. and M.M.; writing—original draft, V.-E.O., A.-I.B., C.C. and A.-M.L.; writing—review and editing, V.-E.O., A.-I.B. and N.P. All authors have read and agreed to the published version of the manuscript.

Conflicts of Interest: The authors declare no conflict of interest.

References

1. Biljecki, F. Level of Detail in 3D City Models. Ph.D Thesis, Delf University of Technology, Delf, The Netherlands, 2017.
2. Jovanović, D.; Milovanov, S.; Ruskovski, I.; Govedarica, M.; Sladić, D.; Radulović, A.; Pajić, V. Building Virtual 3D City Model for Smart Cities Applications: A Case Study on Campus Area of the University of Novi Sad. *ISPRS Int. J. Geo-Inf.* **2020**, *9*, 476. [CrossRef]
3. Kirpes, C.; Hu, G.; Sly, D. The 3D Product Model Research Evolution and Future Trends: A Systematic Literature Review. *Appl. Syst. Innov.* **2022**, *5*, 29. [CrossRef]
4. Bittner, K.; D'Angelo, P.; Körner, M.; Reinartz, P. DSM-to-LoD2: Spaceborne Stereo Digital Surface Model Refinement. *Remote Sens.* **2018**, *10*, 1926. [CrossRef]
5. Poli, D.; Remondino, F.; Angiuli, E.; Agugiaro, G. Radiometric and geometric evaluation of GeoEye-1, WorldView-2 and Pléiades-1A stereo images for 3D information extraction. *ISPRS J. Photogramm. Remote Sens.* **2015**, *100*, 35–47. [CrossRef]
6. Loghin, A.-M.; Otepka-Schremmer, J.; Pfeifer, N. Potential of Pléiades and WorldView-3 Tri-Stereo DSMs to Represent Heights of Small Isolated Objects. *Sensors* **2020**, *20*, 2695. [CrossRef]
7. Oniga, V.-E.; Breaban, A.-I.; Pfeifer, N.; Diac, M. 3D Modeling of Urban Area Based on Oblique UAS Images—An End-to-End Pipeline. *Remote. Sens.* **2022**, *14*, 422. [CrossRef]
8. CityGML: OGC Standards. Available online: https://www.ogc.org/standards/citygml (accessed on 20 March 2022).
9. Ling, X.; Zhang, Y.; Xiong, J.; Huang, X.; Chen, Z. An Image Matching Algorithm Integrating Global SRTM and Image Segmentation for Multi-Source Satellite Imagery. *Remote Sens.* **2016**, *8*, 672. [CrossRef]
10. Jin, Y.; Mishkin, D.; Mishchuk, A.; Matas, J.; Fua, P.; Yi, K.M.; Trulls, E. Image Matching Across Wide Baselines: From Paper to Practice. *Int. J. Comput. Vis.* **2021**, *129*, 517–547. [CrossRef]
11. Trimble. *Match-T DSM Reference Manual*; Trimble Inc.: Sunnyvale, CA, USA, 2016.
12. Partovi, T.; Fraundorfer, F.; Bahmanyar, R.; Huang, H.; Reinartz, P. Automatic 3-D Building Model Reconstruction from Very High Resolution Stereo Satellite Imagery. *Remote Sens.* **2019**, *11*, 1660. [CrossRef]
13. Perko, R.; Raggam, H.; Roth, P.M. Mapping with Pléiades—End-to-End Workflow. *Remote Sens.* **2019**, *11*, 2052. [CrossRef]
14. Loghin, A.M.; Otepka, J.; Karel, W.; Pöchtrager, M.; Pfeifer, N. Accuracy Analysis of Digital Elevation Models from very High Resolution Satellite Imagery. *Publ. Der DGPF* **2019**, *28*, 123–137.
15. Rieg, L.; Klug, C.; Nicholson, L.; Sailer, R. Pléiades Tri-Stereo Data for Glacier Investigations—Examples from the European Alps and the Khumbu Himal. *Remote Sens.* **2018**, *10*, 1563. [CrossRef]
16. Belart, J.M.C.; Berthier, E.; Magnússon, E.; Anderson, L.S.; Pálsson, F.; Thorsteinsson, T.; Howat, I.M.; Aðalgeirsdóttir, G.; Jóhannesson, T.; Jarosch, A.H. Winter mass balance of Drangajökull ice cap (NW Iceland) derived from satellite sub-meter stereo images. *Cryosphere* **2017**, *11*, 1501–1517. [CrossRef]
17. Wagnon, P.; Vincent, C.; Arnaud, Y.; Berthier, E.; Vuillermoz, E.; Gruber, S.; Ménégoz, M.; Gilbert, A.; Dumont, M.; Shea, J.M.; et al. Seasonal and annual mass balances of Mera and Pokalde glaciers (Nepal Himalaya) since 2007. *Cryosphere* **2013**, *7*, 1769–1786. [CrossRef]
18. Almeida, L.P.; Almar, R.; Bergsma, E.W.J.; Berthier, E.; Baptista, P.; Garel, E.; Dada, O.A.; Alves, B. Deriving High Spatial-Resolution Coastal Topography From Sub-meter Satellite Stereo Imagery. *Remote. Sens.* **2019**, *11*, 590. [CrossRef]
19. Nurtyawan, R.; Fiscarina, N. Assessment of the Accuracy of Dem from Panchromatic Pleiades Imagery (Case Study: Bandung City. West Java). *Int. J. Remote Sens. Earth Sci. (IJReSES)* **2020**, *17*, 34–44. [CrossRef]
20. Stumpf, A.; Malet, J.-P.; Allemand, P.; Ulrich, P. Surface reconstruction and landslide displacement measurements with Pléiades satellite images. *ISPRS J. Photogramm. Remote. Sens.* **2014**, *95*, 1–12. [CrossRef]
21. Ok, A.O.; Ozdarici-Ok, A.; Baseski, E. Accuracy Assessment of Pleiades-1 Stereo/Tri-stereo Digital Surface Models: A Case-Study for Citrus Trees. *J. Indian Soc. Remote Sens.* **2018**, *46*, 1203–1212. [CrossRef]
22. Palaseanu-Lovejoy, M.; Bisson, M.; Spinetti, C.; Buongiorno, M.F.; Alexandrov, O.; Cecere, T. High-Resolution and Accurate Topography Reconstruction of Mount Etna from Pleiades Satellite Data. *Remote Sens.* **2019**, *11*, 2983. [CrossRef]
23. Panagiotakis, E.; Chrysoulakis, N.; Charalampopoulou, V.; Poursanidis, D. Validation of Pleiades Tri-Stereo DSM in Urban Areas. *ISPRS Int. J. Geo-Inf.* **2018**, *7*, 118. [CrossRef]
24. Tripodi, S.; Duan, L.; Poujade, V.; Trastour, F.; Bauchet, J.-P.; Laurore, L.; Tarabalka, Y. Operational Pipeline for Large-scale 3D Reconstruction of Buildings from Satellite Images. In Proceedings of the IGARSS 2020-IEEE International Geoscience and Remote Sensing Symposium, Big Island, HI, USA, 26 September–2 October 2020.
25. Flamanc, D.; Maillet, G. *Evaluation of 3D City Model Production from Pléiades Hr Satellite Images and 2D Ground Maps*; URBAN: Tempe, AZ, USA, 2005.
26. Abduelmula Abdunaser, E. High Resolution Satellite Image Analysis and Rapid 3D Model Extraction for Urban Change Detection. PhD. Thesis, Faculty of Science University of Porto, Porto, Portugal, June 2015.

27. Pepe, M.; Costantino, D.; Alfio, V.S.; Vozza, G.; Cartellino, E. A Novel Method Based on Deep Learning, GIS and Geomatics Software for Building a 3D City Model from VHR Satellite Stereo Imagery. *ISPRS Int. J. Geo-Inf.* **2021**, *10*, 697. [CrossRef]

28. d'Angelo, P.; Kuschk, G. Dense multi-view stereo from satellite imagery. In Proceedings of the 2012 IEEE International Geoscience and Remote Sensing Symposium, Munich, Germany, 22–27 July 2012; pp. 6944–6947.

29. Remondino, F.; Spera, M.G.; Nocerino, E.; Menna, F.; Nex, F.C. State of the art in high density image matching. *Photogramm. Rec.* **2014**, *29*, 144–166. [CrossRef]

30. Alobeid, A.; Jacobsen, K.; Heipke, C. Comparison of Matching Algorithms for DSM Generation in Urban Areas from Ikonos Imagery. *J. Photogramm. Eng. Remote Sens.* **2010**, *76*, 1041–1050. [CrossRef]

31. Alobeid, A. *Assessment of Matching Algorithms for Urban DSM Generation from Very High Resolution Satellite Stereo Images*; Scientific Papers Specializing in Geodesy and Geoinformatics at Leibniz Universität Hannover; Leibniz Universität Hannover: Hanover, Germany, 2011; ISSN 0174-1454.

32. Iurist (Dumitrascu), N.-V.; Oniga, E.-V.; Statescu, F. Comparative study on digital terrain models created based on ALS data and Pléiades images. *J. Geod. Cadastre RevCAD* **2015**, *19*, 127–134.

33. Piermattei, L.; Marty, M.; Karel, W.; Ressl, C.; Hollaus, M.; Ginzler, C.; Pfeifer, N. Impact of the acquisition geometry of Very High-Resolution Pléiades imagery on the accuracy of canopy height models over forested alpine regions. *Remote Sens.* **2018**, *10*, 1542. [CrossRef]

34. Sofia, G.; Bailly, J.-S.; Chehata, N.; Tarolli, P.; Levavasseur, F. Comparison of Pléiades and LiDAR Digital Elevation Models for Terraces Detection in Farmlands. *IEEE J. Sel. Top. Appl. Earth Obs. Remote Sens.* **2016**, *9*, 1567–1576. [CrossRef]

35. Baybura, T.; Tiryakioğlu, İ.; Uğur, M.A.; Solak, H.İ.; Şafak, Ş. Examining the accuracy of network RTK and long base RTK methods with repetitive measurements. *J. Sens.* **2019**, *2019*, 3572605. [CrossRef]

36. Elaksher, A.; Ali, T.; Kamtchang, F.; Wegmann, C.; Guerrero, A. Performance analysis of multi-GNSS static and RTK techniques in estimating height differences. *Int. J. Digit. Earth* **2020**, *13*, 586–601. [CrossRef]

37. Van Sickle, J. *GPS for Land Surveyors*; CRC Press: Boca Raton, FL, USA, 2008.

38. Romanian Position Determination System: Real Time Products. Available online: https://rompos.ro/index.php/en/technical-info/real-time-products (accessed on 20 April 2022).

39. US Army Corps of Engineers. Engineering and Design. Control and Topographic Surveying, 2007, Engineer Manual, Department of the Army EM 1110-1-1005, CECW-CE Washington, DC 20314-1000. Available online: https://www.publications.usace.army.mil/Portals/76/Publications/EngineerManuals/EM_1110-1005.pdf?ver=7p8yphfzUR5LZG5faL9R9A%3d%3d (accessed on 20 April 2022).

40. Lin, L.S. Orthometric Height Improvement in Tainan City Using RTK GPS and Local Geoid Corrector Surface Models. *J. Surv. Eng.* **2013**, *140*, 35–43. [CrossRef]

41. Dragomir, P.I.; Rus, T.; Avramiuc, N.; Dumitru, P. EVRF2007 as Realization of the European Vertical Reference System (EVRS) in Romania. *RevCAD–J. Geod. Cadastre* **2011**, *11*, 51–63.

42. *Help TransDatRO: User Guide*; National Agency for Cadastre and Land Registration; National Center for Cartography: Bucharest, Romania, 2022; Available online: https://cngcft.ro/index.php/ro/download/download/2-software/7-transdatro-4-07 (accessed on 20 April 2022).

43. Featherstone, W.E. GNSS-Based Heighting in Australia: Current, Emerging and Future Issues. *J. Spat. Sci.* **2018**, *53*, 115–133. [CrossRef]

44. Airbus Pléiades Imagery User Guide. Available online: https://www.intelligence-airbusds.com/automne/api/docs/v1.0/document/download/ZG9jdXRoZXF1ZS1kb2N1bWVudC01NTY0Mw==/ZG9jdXRoZXF1ZS1maWxlLTU1NjQy/airbus-pleiades-imagery-user-guide-15042021.pdf (accessed on 1 August 2022).

45. Orfeo Toolbox. Available online: https://www.orfeo-toolbox.org/ (accessed on 8 February 2022).

46. Chirila, C.; Oniga, V.E.; Dumitru, P.D. Quasigeoid fitting to the GNSS/levelling benchmarks in Iasi city area. In Proceedings of the 14th International Multidisciplinary Scientific Geoconference SGEM 2014, Geodesy and Mine Surveying, Conference Proceedings, II, Albena, Bulgaria, 17–26 June 2014; pp. 411–418.

47. Fotopoulos, G. An Analysis on the Optimal Combination of Geoid, Orthometric and Ellipsoidal Height Data. Ph.D. Thesis, University of Calgary, Calgary, Alberta, 2003.

48. *Surfer User's Guide, Ch.4: Creating Grid Files, 201-307*; Golden Software, LLC: Golden, CO, USA, 2022. Available online: https://downloads.goldensoftware.com/guides/Surfer23UserGuide.pdf (accessed on 20 April 2022).

49. Iliffe, J.; Lott, R. *Datums and Map Projections for Remote Sensing, GIS and Surveying*, 2nd ed.; Whittles Publishing: Scotland, UK, 2008; pp. 128–129.

50. Pfeifer, N.; Mandlburger, G.; Otepka, J.; Karel, W. OPALS—A framework for Airborne Laser Scanning data analysis. *Comput. Environ. Urban Syst.* **2014**, *45*, 125–136. [CrossRef]

51. Pfeifer, N.; Mandlburger, G. Filtering and DTM Generation. In *Topographic Laser Ranging and Scanning: Principles and Processing*; Shan, J., Toth, C., Eds.; CRC Press: Boca Raton, FL, USA, 2008; pp. 307–333, ISBN 9781420051421.

52. Zhang, W.; Qi, J.; Wan, P.; Wang, H.; Xie, D.; Wang, X.; Yan, G. An Easy-to-Use Airborne LiDAR Data Filtering Method Based on Cloth Simulation. *Remote Sens.* **2016**, *8*, 501. [CrossRef]

53. Geospatial. Trimble Inpho Brochure. Available online: http://www.inpho.de (accessed on 31 January 2022).

54. Förstner, W. A feature based correspondence algorithm for image matching. *Int. Arch. Photogramm.* **1986**, *26*, 150–166.

55. Biljecki, F.; Ledoux, H.; Stoter, J. Height references of CityGML LOD1 buildings and their influence on applications. In Proceedings of the ISPRS 3D GeoInfo 2014 Conference, Dubai, United Arab Emirates, 11–13 November 2014. [CrossRef]

56. Yu, D.; Ji, S.; Liu, J.; Wei, S. Automatic 3D building reconstruction from multi-view aerial images with deep learning. *ISPRS J. Photogramm. Remote. Sens.* **2021**, *171*, 155–170. [CrossRef]